Original Article

MOLECULAR METABOLISM

# Moderate SIRT1 overexpression protects against brown adipose tissue inflammation

**Carmen Escalona-Garrido [1,2], Patricia Vázquez [1,2,*], Paula Mera [3,4,7], Sebastián Zagmutt [3,7], Ester García-Casarrubios [1,7], Ana Montero-Pedrazuela [1,5,7], Fernanda Rey-Stolle [6], Ana Guadaño-Ferraz [1,5], Francisco J. Rupérez [6], Dolors Serra [3,4], Laura Herrero [3,4], Maria Jesus Obregon [1], Ángela M. Valverde [1,2,**]**

## ABSTRACT

**Objective:** Metainflammation is a chronic low-grade inflammatory state induced by obesity and associated comorbidities, including peripheral insulin resistance. Brown adipose tissue (BAT), a therapeutic target against obesity, is an insulin target tissue sensitive to inflammation. Therefore, it is necessary to find strategies to protect BAT against the effects of inflammation in energy balance. In this study, we explored the impact of moderate sirtuin 1 (SIRT1) overexpression on insulin sensitivity and β-adrenergic responses in BAT and brown adipocytes (BA) under pro-inflammatory conditions.

**Methods:** The effect of inflammation on BAT functionality was studied in obese *db/db* mice and lean wild-type (WT) mice or mice with moderate overexpression of SIRT1 (SIRT1$^{Tg+}$) injected with a low dose of bacterial lipopolysaccharide (LPS) to mimic endotoxemia. We also conducted studies on differentiated BA (BA-WT and BA-SIRT1$^{Tg+}$) exposed to a macrophage-derived pro-inflammatory conditioned medium (CM) to evaluate the protection of SIRT1 overexpression in insulin signaling and glucose uptake, mitochondrial respiration, fatty acid oxidation (FAO), and norepinephrine (NE)-mediated-modulation of uncoupling protein-1 (UCP-1) expression.

**Results:** BAT from the *db/db* mice was susceptible to metabolic inflammation manifested by the activation of pro-inflammatory signaling cascades, increased pro-inflammatory gene expression, tissue-specific insulin resistance, and reduced UCP-1 expression. Impairment of insulin and noradrenergic responses were also found in the lean WT mice upon LPS injection. In contrast, BAT from the mice with moderate overexpression of SIRT1 (SIRT1$^{Tg+}$) was protected against LPS-induced activation of pro-inflammatory signaling, insulin resistance, and defective thermogenic-related responses upon cold exposure. Importantly, the decline in triiodothyronine ($T_3$) levels in the circulation and intra-BAT after exposure of the WT mice to LPS and cold was markedly attenuated in the SIRT1$^{Tg+}$ mice. *In vitro* BA experiments in the two genotypes revealed that upon differentiation with a $T_3$-enriched medium and subsequent exposure to a macrophage-derived pro-inflammatory CM, only BA-SIRT1$^{Tg+}$ fully recovered insulin and noradrenergic responses.

**Conclusions:** This study has ascertained the benefit of the moderate overexpression of SIRT1 to confer protection against defective insulin and β-adrenergic responses caused by BAT inflammation. Our results have potential therapeutic value in combinatorial therapies for BAT-specific thyromimetics and SIRT1 activators to combat metainflammation in this tissue.



**Keywords** Brown adipose tissue; Inflammation; Sirtuin 1; Triiodothyronine; Insulin resistance; Uncoupling protein-1

## 1. INTRODUCTION

Current evidence has demonstrated that adipose tissue is a trigger for the obesity-induced chronic low-grade inflammatory state known as metainflammation [1]. Overnutrition alters the functionality of adipocytes and induces the secretion of many pro-inflammatory cytokines, adipokines, and reactive lipid species that negatively impact whole body metabolism [1–3].

Brown adipose tissue (BAT) is currently considered a therapeutic target against obesity due to its capacity to metabolize large amounts

[1]Instituto de Investigaciones Biomédicas Alberto Sols (Centro Mixto CSIC-UAM), 28029 Madrid, Spain [2]Centro de Investigación Biomédica en Red de Diabetes y Enfermedades Metabólicas Asociadas (CIBERdem), 28029 Madrid, Spain [3]Department of Biochemistry and Physiology, School of Pharmacy and Food Sciences, Institut de Biomedicina de la Universitat de Barcelona (IBUB), Universitat de Barcelona, E-08028 Barcelona, Spain [4]Centro de Investigación Biomédica en Red de Fisiopatología de la Obesidad y la Nutrición (CIBERobn), Instituto de Salud Carlos III, E-28029 Madrid, Spain [5]Centro de Investigación Biomédica en Red de Enfermedades Raras (CIBERer), Instituto de Salud Carlos III, E-28029 Madrid, Spain [6]Centro de Metabolómica y Bioanálisis (CEMBIO), Facultad de Farmacia, Universidad San Pablo-CEU, CEU Universitiy, Urbanización Montepríncipe, Boadilla del Monte, 28660, Madrid, Spain

[7] These authors contributed equally to this work.

*Corresponding author. Instituto de Investigaciones Biomédicas Alberto Sols CSIC-UAM, C/ Arturo Duperier 4, 28029 Madrid Spain. E-mail: patrivazquez@iib.uam.es (P. Vázquez).

**Corresponding author. Instituto de Investigaciones Biomédicas Alberto Sols CSIC-UAM, C/ Arturo Duperier 4, 28029 Madrid Spain. E-mail: avalverde@iib.uam.es (Á.M. Valverde).

Received July 17, 2020 • Revision received October 2, 2020 • Accepted October 6, 2020 • Available online 10 October 2020

https://doi.org/10.1016/j.molmet.2020.101097

 

of lipids and glucose and dissipate energy as heat in a process known as non-shivering thermogenesis mediated by the mitochondrial uncoupling protein-1 (UCP-1) [4]. The study of BAT has exponentially become more relevant since its re-discovery in adult humans [5–7]. The transcript levels of pro-inflammatory cytokines are lower in BAT than in white adipose tissue (WAT), which probably reflects an enhanced anti-inflammatory phenotype of BAT resident immune cells [8]. However, increased levels of tumor necrosis factor (TNF)-$\alpha$ or interleukin (IL)-1$\beta$ [9–11] as well as insulin resistance [10] and reduced energy expenditure [12] have been reported in BAT from rodents under obesogenic conditions. Activation of BAT, either in humans or rodent models, is associated with healthy systemic metabolism [13,14]. In addition, the secretory capacity of BAT was recently attributed to the modulation of its thermogenic capacity [14–16].

Thyroid hormones (THs) are transcriptional activators of the *Ucp1* gene [17,18]. They are also essential to maintain norepinephrine (NE)-mediated signaling in BAT by improving thermogenesis in brown adipocytes (BA) [19–21]. A recent study demonstrated a dual effect of triiodothyronine ($T_3$) in inguinal WAT (iWAT) in which it cooperates with $\beta$-adrenergic signaling to induce the transcription of the *Ucp1* gene in a cAMP-dependent manner and also activates *de novo* lipogenesis independently of cAMP signaling [22]. Thyromimetics that specifically target BAT may be useful for its pharmacological activation [23]. Yau *et al.* [24] extended the knowledge on the cell autonomous actions of $T_3$ in BA demonstrating its effects in increasing fatty acid oxidation (FAO) and mitochondrial respiration. Other studies reported the impact of inflammation on THs actions by administering bacterial lipopolysaccharide (LPS) to mice or pigs, which decreases the expression of THs receptors in the heart [25] or THs levels in the serum and most tissues [26]. The anti-inflammatory effect of THs was also reported in humans [27].

Sirtuins are $NAD^+$-dependent protein deacetylases involved in fundamental biological processes such as development, metabolism, aging, and associated diseases [28–31]. Several studies revealed the beneficial effects of overexpressing the family member SIRT1 in metabolic disorders. Because SIRT1 is an essential regulator of systemic energy homeostasis, its pharmacological modulation could be of interest to control diseases associated with metainflammation [32]. In this sense, the moderate overexpression of SIRT1 in mice deacetylates the RelA/p65 subunit of nuclear factor kappa B (NF$\kappa$B) and inhibits its activity in the liver, thereby attenuating inflammatory responses in diet-induced obesity [33], supporting its anti-inflammatory role. Moreover, browning of white adipocytes upon cold exposure was reported in another model of SIRT1 transgenic mice (SirBACO) [34] or in mice with genetic deletion of the SIRT1 endogenous inhibitor deleted in breast cancer 1 (*Dbc1*$^{-/-}$) [35]. We previously reported enhanced BAT activity in mice with constitutive SIRT1 overexpression (SIRT1$^{Tg/Tg}$ mice) on a low-fat diet, supporting a higher catabolic rate [36]. Conversely, SIRT1-deficient mice showed the opposite effect with exacerbated BAT degeneration, cold and glucose intolerance, and insulin resistance in response to a high-fat diet (HFD) [37].

In the present study, we provided evidence that the moderate overexpression of SIRT1 is sufficient to confer protection against defective insulin and $\beta$-adrenergic responses caused by BAT inflammation. Of note, this protection was associated with increased $T_3$ content in this fat depot. The beneficial effects of SIRT1 overexpression were also assessed in a cell-autonomous manner in BA and full protection against the deleterious effect of inflammation was achieved in cells differentiated with a $T_3$-enriched medium.

## 2. MATERIALS AND METHODS

### 2.1. Animal studies

All animal procedures were approved by the Ethics Committees of the Spanish National Research Council of Madrid (Spain) in accordance with the European Union's guidelines. *Db*+ and *db/db* male and female mice with C57BL/KsJ genetic backgrounds were purchased from Charles Rivers Laboratories. C57Bl/6J mice overexpressing SIRT1 (SIRT1$^{Tg+}$) were provided by Dr. Manuel Serrano (CNIO, Madrid). Mice were housed at the animal facilities at Instituto de Investigaciones Biomédicas (IIBm) Alberto Sols (CSIC/UAM, Madrid) under controlled conditions of 12 h:12 h light–dark cycles at 22 °C and 45–55% humidity and allowed free access to a standard rodent chow diet (A04, U8220G10R, SAFE) and water.

The *Db*+ and *db/db* mice (males and females, 7 weeks of age) were treated with resveratrol (R5010, Sigma–Aldrich) for 8 weeks. The resveratrol was dissolved in their drinking water to a final concentration of 50 mg/L and protected from light as previously described [38]. The resveratrol dose was equivalent to approximately 2.5 mg/kg/day. During our study, we confirmed that the mice were consuming the amount of water necessary to reach the desired pharmacological resveratrol dose [39]. Their body weights and glycemia were monitored weekly.

Wild-type (WT) and SIRT1$^{Tg+}$ male mice (2–5 months of age) were fasted for 5 h and then intraperitoneally (i.p.) injected with 2 mg/kg lipopolysaccharide (LPS, tlrl-eblps, InvivoGen) or saline (vehicle). The mice were sacrificed at different time periods ranging from 30 min to 1 h to assess the activation of the pro-inflammatory signaling cascades in BAT. One group of animals was maintained under control conditions (22 °C) without receiving LPS (-LPS). The other 2 groups were injected with 2 mg/kg LPS (i.p.) and sacrificed after 30 min, 60 min, or 4 h (LPS 30 min, LPS 60 min, and LPS 4 h, respectively).

To analyze their *in vivo* insulin responses, the mice (*db*+, *db/db*, WT, and SIRT1$^{Tg+}$) were fasted for 4 h, i.p. injected with 0.75 U/kg of human recombinant human insulin (Actrapid, Novo Nordisk), and sacrificed 20 min later. To analyze their insulin responses under pro-inflammatory conditions, the WT and SIRT1$^{Tg+}$ mice were injected with 2 mg/kg LPS (i.p.) for 24 h and fasted for the last 4 h. The control group did not receive LPS. After 24 h, the mice were injected with 0.75 U/kg of insulin (i.p.) and sacrificed after 20 min. A subgroup of mice did not receive insulin injections.

To analyze their thermogenic responses, the WT and SIRT1$^{Tg+}$ mice were housed at 28 °C for one week and then subjected to a cold challenge (4 °C) for 6 h. To analyze the effect of LPS and cold exposure, the WT and SIRT1$^{Tg+}$ mice were i.p. injected with 2 mg/kg of LPS and sacrificed after 24 h. One subgroup of mice was exposed to the cold during the last 6 h.

All mice were sacrificed and their BAT and different fat depots were weighed and stored at −80 °C until use. Blood was collected by beheading in tubes with 20 mM of ethylenediaminetetraacetic acid (EDTA).

### 2.2. Measurement of rectal and skin temperature surrounding BAT

Rectal temperature was measured with a rectal probe (RTC-1, Cibertec). The skin temperature surrounding BAT was recorded with an infrared camera (B335 compact infrared thermal imaging camera, FLIR Systems, West Malling, Kent, UK) and analyzed with a software package (FLIR Tools Software, FLIR Systems). Images were captured and the temperature was measured at 28 °C or immediately after cold exposure (6 h). In the mice injected with LPS, the measurements were recorded 24 h after the injection.

 

### 2.3. Radioimmunoassays of $T_3$ and $T_4$ in plasma and BAT

Extraction of $T_3$ and $T_4$ from plasma or BAT tissue as well as $T_3$ and $T_4$ determinations in plasma was conducted as previously described [40]. (3—5)-$T_2$ (D0629, Sigma—Aldrich) and $T_3$ (T2877, Sigma—Aldrich) were used as substrates to obtain high specific activity (3000 μCi/μg) $^{125}$I-$T_3$ and $^{125}$I-$T_4$, respectively, using $^{125}$I (NEZ033A, PerkinElmer) as previously described [41,42] with minor modifications [43]. THs from plasma were extracted with methanol (1:6), subjected to evaporation, and resuspended in radioimmunoassay (RIA) buffer (0.04 M of phosphate buffer and pH 8), with 0.2% bovine serum albumin (BSA) and 0.6 mM of merthiolate (T-5125, Sigma—Aldrich). For the extraction and purification of THs from BAT, frozen tissue samples (70—100 mg) were homogenized in methanol. THs were extracted using chloroform-methanol (2:1), back-extracted into an aqueous phase, and purified using AG 1-X2 resin (1401251, Bio-Rad) in custom-made columns using a pH gradient. The acetic extracts were then evaporated to dryness and dissolved in RIA buffer. The extracts were kept frozen until further analysis by highly sensitive RIA to determine $T_3$ and $T_4$ (dynamic range: 0.4—100 pg $T_3$/tube and 2.5—320 pg $T_4$/tube). The radioactivity was quantified in a gamma counter (Cobra II B5003, Packard). The concentrations were calculated using the amounts of $T_3$ and $T_4$ detected in the RIAs. The recovery of the [$^{125}$I]-$T_4$ and [$^{125}$I]-$T_3$ was added to tracer samples, and the weights of the tissue samples were extracted.

### 2.4. Histological analysis and immunostaining

Hematoxylin and eosin (H&E) staining was performed in paraffin sections of BAT from the WT and SIRT1$^{Tg+}$ mice. BAT tissue was fixed in 4% paraformaldehyde (PFA, 16005, Sigma—Aldrich) for 24 h, washed twice with PBS, dehydrated with ascending ethanol solutions, incubated with xylene, and then embedded in paraffin. Blocks were cut into 5 μm sections. Prior to H&E staining or immunohistochemistry, the sections were deparaffinized in xylene and hydrated in descending ethanol solutions and distilled water. The slides were stained with Mayer's hematoxylin (MHS32-1L, Sigma—Aldrich) for 15—20 min and eosin (1.15935.0025, Merck) for 1 min. After the slides were dried and mounted, the images were captured with an Axiophot light microscope (Zeiss) using a 40× objective. To estimate the cell density, the nuclei were counted in 3 fields of different BAT sections of each animal using ImageJ software (National Institutes of Health; https://imagej.nih.gov/ij/). Approximately 200 total nuclei per section were counted.

For UCP-1 immunohistochemistry, sections were heated for 20 min in 100 mM of sodium citric buffer (pH 6.0) and 0.05% Tween-20. After washing with PBS, endogenous peroxidase was blocked by incubation with a solution of 9% $H_2O_2$ in 10% methanol for 10 min at room temperature. The tissue sections were then incubated in 6% BSA and 2% normal horse serum (NHS) in PBS-0.1% Triton X-100 for 1 h at room temperature to block non-specific binding. The sections were incubated with primary antibody against UCP-1 (1:500, Ab10983, Abcam) overnight at 4 °C. The sections were washed with PBS and incubated with biotinylated secondary anti-rabbit (1:250) (BA-1100, Vector Laboratories) for 1 h at room temperature. After washing with PBS, the slides were incubated with DAB-immunoperoxidase staining (SK-4100, Vector Laboratories). After washing with water for 5 min, the sections were counterstained with hematoxylin (H3136, Sigma—Aldrich) solution for 10 s and rinsed again with water. After dehydration and xylene incubation, the sections were assembled with DePeX (18243.02, SERVA Electrophoresis GmbH), covered with coverslips, and dried overnight.

### 2.5. Differentiation of immortalized brown preadipocyte cell lines from the WT and SIRT1$^{Tg+}$ mice

WT and SIRT1$^{Tg+}$ brown preadipocyte cell lines were generated as previously described [36]. The detailed protocol is described in the Supplementary Materials and Methods section. Immortalized preadipocytes were maintained in DMEM supplemented with 100 U/mL penicillin, 100 μg/mL streptomycin, 10 mM HEPES, and 10% FBS. Cells were plated in DMEM supplemented with 10% FBS, 1 nM of $T_3$ (T6397, Sigma—Aldrich), and 20 nM of insulin. This medium was called medium 1. For differentiation, the cells were grown until 90% confluence followed by two differentiation protocols.

In protocol 1, cells were stimulated for 36 h with differentiation medium 1 containing medium 1 supplemented with 0.5 μM of dexamethasone (D1756, Sigma—Aldrich), 1 μM of rosiglitazone (R2408, Sigma—Aldrich), 0.5 mM of isobutylmethylxanthine (IBMX) (I5879, Sigma—Aldrich), and 0.125 μM of indomethacin (I7378, Sigma—Aldrich). The cells were then cultured back into medium 1 for 3 more days.

In protocol 2, cells were stimulated for 36 h with differentiation medium 2 containing medium 1 supplemented with 35 nM of dexamethasone, 10 μM of rosiglitazone, 2.99 μM of $T_3$, and 830 nM of insulin. The cells were then maintained in DMEM supplemented with 10% FBS, 10 μM of rosiglitazone, 3 μM of $T_3$, and 850 nM of insulin for 3 days (called medium 2). This protocol was adapted from [44]. Differentiated brown adipocytes (BA) were called BA-WT and BA-SIRT1$^{Tg+}$.

### 2.6. Production of pro-inflammatory conditioned medium by macrophages

The murine macrophage cell line Raw 267.4 was used to obtain a pro-inflammatory conditioned medium (CM). The Raw 264.7 cells were maintained in 10 cm culture dishes with Roswell Park Memorial Institute (RPMI) medium supplemented with 100 U/mL of penicillin, 100 μg/mL of streptomycin, 10 mM of HEPES, 2 mM of L-glutamine, and 10% FBS. Macrophages were grown until 95—100% confluence was reached. Then the medium was changed to RPMI-2% FBS for 1 h and the macrophages were treated with 100 ng/mL of LPS for 5 h or left untreated. The culture medium was then removed and the cells were washed with phosphate-buffered saline (PBS) and cultured in RPMI-2% FBS medium for 17 h (referred as CM-LPS or CM-CTR, respectively). Both CM were filtered and supplemented with FBS (final 5%) before the addition of BA. Aliquots of each CM (CM-LPS or CM-CTR) were collected and mixed with 1 mM of sulfanilic acid (151057.1208, Panreac) and 1 mM of N-(l-naphthyl) ethylenediamine (NEDA) (N912510G, Sigma—Aldrich). Nitrite production was measured spectrophotometrically at 548 nM and the concentration was determined using a standard $NO_2$ curve.

### 2.7. Insulin signaling in brown adipocytes

To analyze the insulin signaling in differentiated BA, cells were serum-starved for 1 h in DMEM following stimulation with 10 nM of insulin for 15 min. To assess the insulin response under pro-inflammatory conditions, BA were treated with CM-CTR or CM-LPS for 17 h. After serum starvation for 1 h in DMEM, the cells were stimulated with 10 nM of insulin for 15 min. At the end of the treatments, the cells were lysed and processed.

### 2.8. Measurement of glucose uptake in brown adipocytes

Differentiated BA were treated with CM-CTR or CM-LPS for 17 h and after the cells were serum deprived for 1 h. The cells were then washed twice with Krebs—Ringer phosphate buffer (KRP) (135 mM of

 

NaCl, 5.4 mM of KCl, 1.4 mM of $CaCl_2$, 1.4 mM of $MgSO_4$, 10 mM of sodium pyrophosphate, and pH 7.4) and incubated with KRP buffer for 15—30 min at 37 °C. After stimulation with 10 nM of insulin for 10 min, 2-deoxy-D [$^{1-3}$H] glucose (500 nCi/mL) was added for 5 more min. Control cells were maintained in the absence of insulin stimulation. The cells were washed twice with KRP buffer and solubilized with a syringe in 1% (p/v) SDS. After 2 h of incubation at 37 °C, the radioactivity was measured by liquid scintillation counting. Total protein was determined by the BCA method and the results were normalized to the protein amount in each culture plate.

### 2.9. Analysis of thermogenic responses in brown adipocytes

To analyze the UCP-1 expression in BA, cells were differentiated with protocols 1 or 2. Once differentiated, BA were cultured in DMEM supplemented with 5% FBS for 1 h and then stimulated with 5 μM of norepinephrine (NE, A9512, Sigma—Aldrich) for 17 h or left untreated. To study the impact of a pro-inflammatory environment on the thermogenic responses, BA were cultured with CM-CTR or CM-LPS in the absence or presence of 5 μM of NE for 17 h. At the end of the treatments, the cells were lysed and processed.

### 2.10. Measurement of bioenergetic profile

The oxygen consumption rate (OCR) was measured in BAT explants from the WT and SIRT1$^{Tg+}$ mice. The mice were injected with 2 mg/kg of LPS 24 h before the OCR analyses. The control mice did not receive LPS. BAT was excised and cut using a scalpel into 9 mg pieces and placed into a tube containing DMEM supplemented with 25 mM of glucose and 25 mM of Hepes. Tissues were kept in this medium (wash medium) until the measurement of respiration. The capture screens (Seahorse Bioscience, North Billerica, MA, USA) were pre-wet in wash medium in a small petri dish to remove air bubbles. A pair of sterile forceps was used to position the screens (ring facing up) in a new empty small petri dish, and 9 mg of BAT was placed on the screen using the forceps. The capture screen insert tool (Seahorse Bioscience) was used to pick up the tissue-containing screens from the petri dish and place them in an XF24 Islet Capture Microplate (Seahorse Bioscience). Once in position, 450 μL of assay medium (DMEM supplemented with 25 mM of glucose) was added to the samples. For a typical bioenergetic profile, a set of inhibitors (all from Sigma—Aldrich) of key components of cellular respiration was added: 24 μg/mL of oligomycin A, 0.8 μM of FCCP uncoupler, and a mix of 5 μM of rotenone and 15 μM of antimycin A for BAT explants.

To analyze the OCR in BA, cells were differentiated with medium 1 or 2 in customized Seahorse 24-well plates and stimulated with CM-CTR and CM-LPS for 18 h. Before any measurement, the cells were incubated for 1 h with XF Assay Medium (Seahorse Bioscience) plus 5 mM of glucose. We followed the protocol and injection strategies of the Mito Stress Assay (Seahorse Bioscience). The concentrations of the inhibitors were 2 μM of oligomycin (75351, Sigma—Aldrich), 2 μM of FCCP uncoupler (C2920, Sigma—Aldrich), and a mix of 10 μM of rotenone (R8875, Sigma—Aldrich) and 10 μM of antimycin-A (A8674, Sigma—Aldrich) for mature BA.

The OCR was calculated by plotting the $O_2$ tension of media as a function of the time (pmol/min), and the data were normalized by the protein concentration measured in each individual well using Bradford's method. Calculations were conducted as previously described [45] using Agilent Seahorse Wave Desktop software.

### 2.11. Fatty acid oxidation (FAO) analysis

Palmitate oxidation to $CO_2$ and acid-soluble products (ASPs), essentially acyl-carnitine, Krebs cycle intermediates, and acetyl-CoA, was measured in BA-WT and BA-SIRT1$^{Tg+}$ grown and differentiated in 24-well plates. The day of the assay, the cells were washed in Krebs—Ringer bicarbonate Hepes buffer (KRBH buffer: 135 mM of NaCl, 3.6 mM of KCl, 0.5 mM of $NaH_2PO_4$, 0.5 mM of $MgSO_4$, 1.5 mM of $CaCl_2$, 2 mM of $NaHCO_3$, 10 mM of HEPES, and pH 7.4) and 0.1% of BSA, preincubated at 37 °C for 30 min in KRBH-1% BSA, and washed again in KRBH-0.1% BSA. The cells were then incubated for 3 h at 37 °C with fresh KRBH containing 25 mM of glucose, 8 mM of carnitine (C0283, Sigma—Aldrich), 2.5 mM of palmitate, and 1 μCi/mL of [1—$^{14}$C] palmitate (CFA23, Amersham Pharmacia Biotech) bound to BSA. Oxidation measurements were conducted as previously described [46] with minor modifications by trapping the radioactive $CO_2$ in a 1 $cm^2$ Whatman paper soaked with 100 μL of 0.1 N KOH using a parafilm-sealed system. The reaction was stopped by adding 40% perchloric acid through a syringe that pierced the parafilm. The following day, the system was opened and the papers were left to dry before transferring them into tubes with 5 mL of scintillation liquid (6013159, Perkin Elmer). Then 300 μL of the reaction mix with perchloric acid was removed and centrifuged at the maximum speed for 10 min. Then 150 μL of the supernatant that contained the ASPs was transferred into a tube containing 5 mL of scintillation liquid. After 2 h of stabilization, the samples were analyzed and the $CO_2$ data were expressed as nmol palmitate $mg^{-1}$ prot * $h^{-1}$ = ($cpm_{sample}$ - $cpm_{blanc}$) * 80/(total cpm * mg prot * h). The ASP results were expressed as nmol palmitate $mg^{-1}$ prot * $h^{-1}$ = ($cpm_{sample}$ - $cpm_{blanc}$) * 80 * (352/150)/(total cpm * mg prot * h) as previously described [46].

### 2.12. Analysis of protein expression by Western blotting

The detailed protocols for the protein analysis are described in the Supplementary Materials and Methods section.

### 2.13. Semi-quantitative and quantitative real-time PCR analysis

The detailed protocols for the real-time PCR analysis are described in the Supplementary Materials and Methods section.

### 2.14. Analysis of mitochondrial markers by immunofluorescence

BA were differentiated with medium 1 or 2 in sterile round glass coverslips and fixed with 4% PFA at pH 7.5 for 20 min at room temperature. After washing with PBS, the cells were permeabilized with 0.1% sodium citrate at pH 6 and 0.1% Triton X-100 for TOM 22 and COX-IV immunofluorescence or with 0.1% Triton X-100 in PBS for MFN2 and p-DRP1 immunofluorescence for 5 min at room temperature. After washing with washing buffer (0.25% BSA and 0.1% Tween-20 in PBS) for 10 min, the cells were blocked for 30 min at room temperature with 2.4% BSA in washing solution for TOM 22 and COX-IV or with 5% normal goat serum (NGS, ab7481, Abcam) and 5% BSA in PBS for MFN2 and p-DRP1. The cells were then incubated with primary antibodies ((TOM 22, (T6319, Sigma—Aldrich), COX-IV (1D6EIA9, Thermo Fisher Scientific), p-DRP1 (3455, Cell Signaling), or MFN2 (ab56889, Abcam)) at 1:200 dilution in blocking solution overnight at 4 °C and the incubation continued the following day for 30 min at room temperature. After washing twice with PBS, the cells were incubated with fluorochrome-conjugated secondary antibodies ((goat anti-rabbit Alexa 488 (A11034, Thermo Fisher Scientific) for TOM 22, goat anti-mouse Alexa 488 (A11029, Thermo Fisher Scientific) for COX-IV), goat anti-rabbit Alexa 647 (A21245, Thermo Fisher Scientific) for p-DRP1, and goat anti-mouse Alexa 488 (A11029, Thermo Fisher Scientific) for MFN2)) at 1:250 dilution in blocking buffer with DAPI (1 μg/mL, 62248, Thermo Fisher Scientific) for 1 h at room temperature. Coverslips were adhered with antifade mounting medium

 

(00-4958-02, Thermo Fisher Scientific), allowed to dry overnight, and then maintained at 4 °C until confocal microscopy analysis.

### 2.15. Staining of lipid droplets with Bodipy

BA were differentiated with medium 1 or 2 and incubated with 1–5 μg/mL of Bodipy dye (D3835, Thermo Fisher Scientific) dilution for 30 min at 37 °C. The cells were washed twice with PBS, fixed with 4% PFA at pH 7.5 for 20 min at room temperature, and then incubated with DAPI (1 μg/mL) for 5 min at room temperature. Coverslips were adhered with antifade mounting medium, allowed to dry overnight, and then maintained at 4 °C until confocal microscopy analysis.

### 2.16. Flow cytometry

BA were incubated with 100 nM of MitoTracker Green (MTG, M7514, Thermo Fisher Scientific) for 30 min at 37 °C. After washing with PBS, the cells were trypsinized, neutralized, and centrifuged at 238 × *g*. The pellet was resuspended in PBS and the relative MTG fluorescence was determined by flow cytometry (FACSCanto, Becton Dickinson) and FACS Diva (Becton Dickinson) software.

### 2.17. Lipolysis assay

BA were stimulated for 18 h with DMEM-5% FBS and then incubated with Krebs–Ringer Modified Buffer (KRB) (118.5 mM of NaCl, 4.75 mM of KCl, 1.92 mM of $CaCl_2$, 1.19 mM of $KH_4PO_4$, 1.19 mM of $MgSO_4(H_2O)_7$, 25 mM of $NaHCO_3$, 10 mM of HEPES, 6 mM of D-glucose, 4% BSA, and pH 7.4) and 5 μM of NE was added for the last 4 h. Supernatants were collected and the amount of glycerol was quantified spectrophotometrically at 540 nm with a Free Glycerol Reagent colorimetric kit (12812, BioSystems). The amount of glycerol was determined using a commercial standard solution and normalized to the protein amount of each sample.

### 2.18. Measurement of ATP levels

Cells were lysed in cold Milli-Q water, heated to 80 °C for 5 min, and centrifuged at 134 × *g* for 5 min. The ATP levels were detected using a bioluminescence kit (ATP determination kit, PRO (LBR-PO10)) following manufacturer's instructions (Biaffin GMbH & Co. KG). The chemiluminescence generated was detected at a 560 nm wavelength in a luminometer (GloMax 96 Microplate Luminometer, 9101-002, Promega). A curve with increasing concentrations of ATP was used to calculate the amount of ATP in each sample.

### 2.19. GC/MS-targeted metabolomics

Metabolomic studies are described in the Supplementary Materials and Methods section.

### 2.20. Analysis of FGF21 plasma levels

FGF21 plasma levels were quantified by ELISA (RD291108200R, BioVendor) following the manufacturer's instructions. Samples were collected from the *db*+ and *db/db* mice treated with resveratrol or not for 8 weeks and after 4 h of fasting.

### 2.21. Statistical analysis

Statistical analysis was conducted using GraphPad Prism software versions 5 and 8 (GraphPad Software Inc., San Diego, CA, USA). The D'Agostino-Pearson omnibus normality test was run to determine if the samples showed a parametric or non-parametric distribution. Mann–Whitney U test was used to conduct pairwise comparisons in the non-parametric distributions. Two-way ANOVA with Bonferroni's post hoc test was employed to compare two different categorical independent variables. The data are presented as mean ± SEM (standard error of the mean). Statistical significance was set at $^{*,\#}p < 0.05$, $^{**,\#\#}p < 0.01$, and $^{***,\#\#\#}p < 0.001$.

## 3. RESULTS

### 3.1. BAT from the *db/db* mice showed activation of pro-inflammatory signaling cascades and reductions in UCP-1 and insulin signaling

We initially conducted studies in the *db/db* mice, a genetic model with key features of obesity, metainflammation, and type 2 diabetes mellitus (T2DM). As previously reported [47,48], the *db/db* mice had obesity and hyperglycemia (Figure. S1A–B) compared to their *db*+ lean counterparts concurrently with higher adiposity (BAT, iWAT, and eWAT) (Figure. S1C–E). Moreover, phosphorylated levels of kinases related to inflammatory states such as STAT3, IKKα/β, JNK, and p38 MAPK were significantly elevated in BAT extracts from the *db/db* mice compared to the *db*+ controls (Figure 1A). This pro-inflammatory signature was also manifested by increased mRNA expression of *Tlr4*, *Il6*, and *Nos2* (Figure 1B). Supporting an impaired BAT function associated with its inflammatory state, the UCP-1 protein content was decreased in the *db/db* mice (Figure 1C).

We next studied whether inflammation impaired insulin signaling in BAT from the *db/db* mice. Our data showed that phosphorylation of IR and AKT was significantly reduced in BAT from the *db/db* mice receiving an i.p. insulin injection (Figure 1D). It is well-known that IR is expressed in cells in two different isoforms containing or not exon 11 (IRB and IRA, respectively) [49]. Although both isoforms have a similar affinity for insulin, IRA is an immature form that exhibits a higher affinity for IGFs. The two IR isoforms were detected in BAT from both groups, but the *db/db* mice showed a robust presence of IRA (Figure 1E) that could account, at least in part, for the attenuated insulin signaling.

### 3.2. Moderate SIRT1 overexpression ameliorated the effects of LPS on BAT inflammation

As endotoxemia is an important component of obesity-induced metainflammation [50], we evaluated whether it is sufficient to activate pro-inflammatory signaling cascades in BAT, an issue less investigated. To achieve this, we mimicked this condition by injecting a low dose of LPS (2 mg/kg) into the wild-type (WT) and mice with a moderate overexpression of SIRT1 ($SIRT1^{Tg+}$) due to their protection against obesity-induced metabolic damage [33]. Figure 2A shows that the SIRT1 protein levels increased (∼threefold) in BAT from the $SIRT1^{Tg+}$ mice. Phosphorylation of STAT3, IKKα/β, JNK, and p38 MAPK rapidly increased in BAT upon LPS challenge; however, the effect on STAT3 and p38 MAPK was ameliorated in the $SIRT1^{Tg+}$ mice (Figure 2B). In addition, the impact of LPS on the elevation of mRNA levels encoding the pro-inflammatory cytokines IL-6 and TNF-α was attenuated in BAT from the $SIRT1^{Tg+}$ mice (Figure 2C).

We determined the impact of LPS-mediated inflammation and moderate SIRT1 overexpression in insulin signaling in BAT. The WT and $SIRT1^{Tg+}$ mice were injected with LPS and after 24 h, a subgroup of animals received an insulin injection. Both genotypes similarly responded to insulin in inducing IR and AKT phosphorylation (Figure S2). Notably, whereas LPS reduced IR and AKT phosphorylation in BAT from the WT mice compared with their genotype counterparts that did not receive LPS (Figure 2D), the $SIRT1^{Tg+}$ mice were protected against the decrease in LPS-mediated insulin signaling. When the 2 genotypes receiving LPS were compared, insulin-induced AKT phosphorylation was significantly increased in the $SIRT1^{Tg+}$ mice (Figure S2).

 

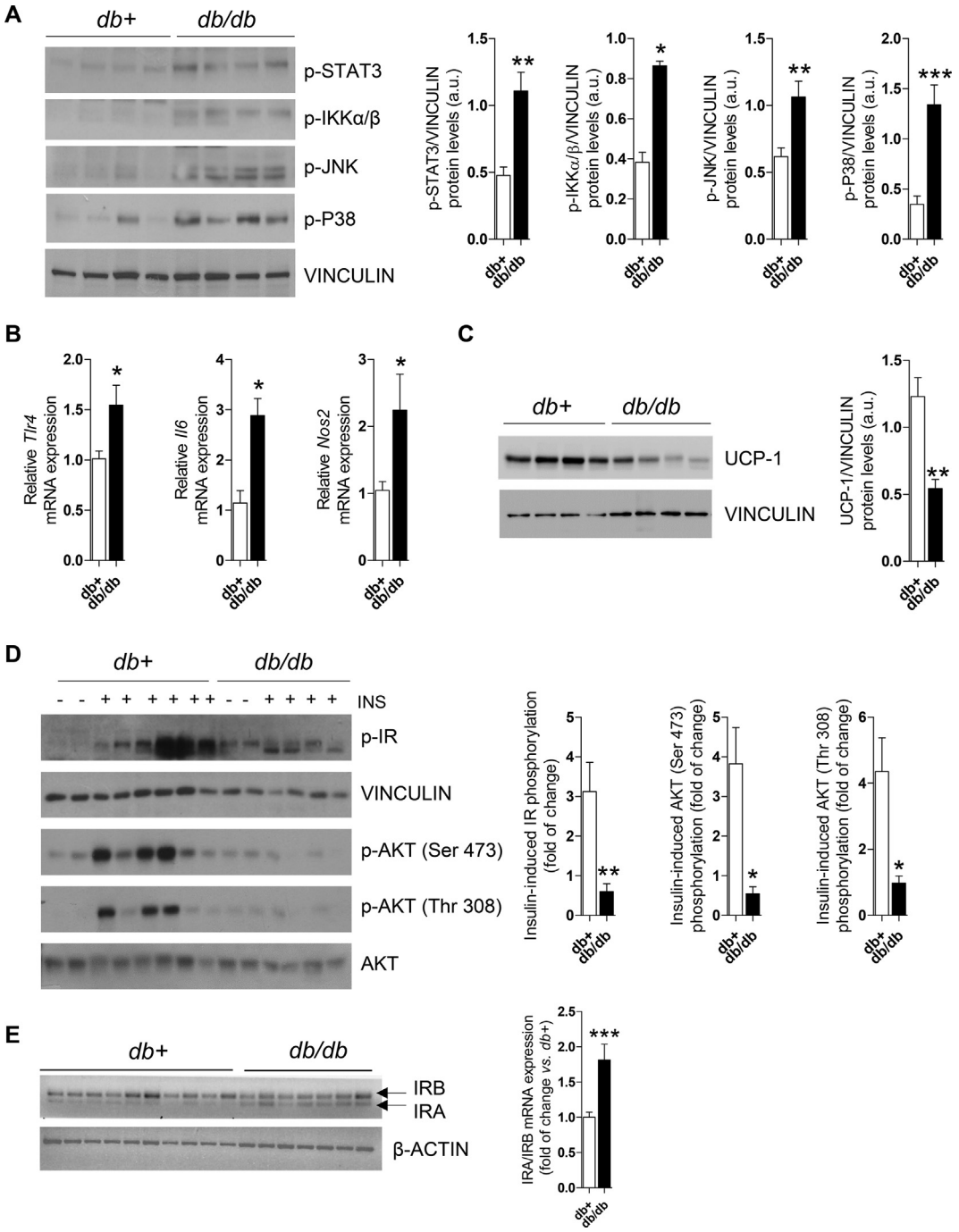


**Figure 1: BAT from the *db/db* mice showed inflammatory features and insulin resistance.** (**A**) Representative Western blotting and quantification of STAT3, IKKα/β, JNK, and p38 MAPK phosphorylation in BAT from the *db*+ and *db/db* mice (n = 4–8 mice/group). (**B**) *Tlr4*, *Il6*, and *Nos2* mRNA expression in BAT (n = 3–7 mice/group). **(C)** Representative Western blotting and quantification of UCP-1 protein levels in BAT (n = 4–7 mice/group). (**D**) Representative Western blotting and quantification of IR and AKT phosphorylation in BAT (n = 2–6 mice/group). (**E**) Pattern of IR isoforms and quantification of the IRA/IRB ratio (n = 7–10 mice/group). Data are expressed as mean ± SEM. The statistical analysis was conducted with the Mann–Whitney U test. $^{*}p < 0.05$, $^{**}p < 0.01$, and $^{***}p < 0.001$.

To study the effects of endotoxemia and moderate SIRT1 overexpression in the thermogenic response of BAT, the mice were housed at 28 °C for one week. One group of each genotype received an LPS injection, and all the groups maintained at 28 °C were sacrificed after 24 h. A slight decrease in the rectal temperature was detected in the LPS-injected WT mice, but not in the SIRT1$^{Tg+}$ mice that also showed higher temperatures in the skin BAT area regardless of the LPS treatment (Figure S3A). Interestingly, histological analysis of BAT sections revealed an increased number of nuclei per field, indicative of higher cell density, in the control or LPS-injected SIRT1$^{Tg+}$ mice compared to the WT mice (Figure S3B). However, although the *Ucp1* mRNA levels were not significantly modulated by LPS, a tendency of

 

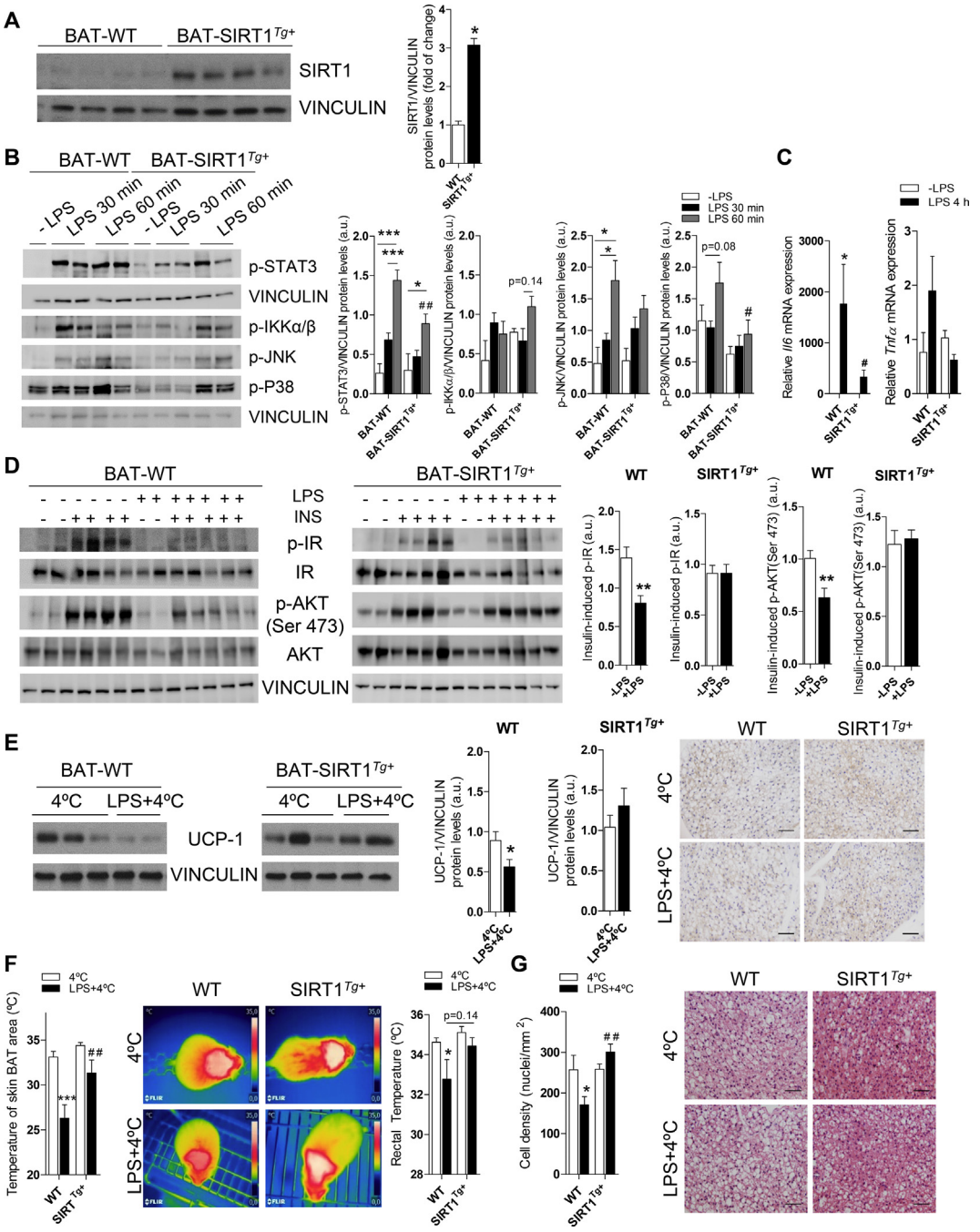


**Figure 2: Moderate SIRT1 overexpression ameliorated the effects of LPS in BAT.** (**A**) Western blotting of SIRT1 in BAT and quantification (n = 4 mice/group). (**B**) Western blotting analysis and quantification of STAT3, JNK, and p38 MAPK phosphorylation in BAT of the WT and SIRT1$^{Tg+}$ mice intraperitoneally (i.p.) injected with LPS (2 mg/kg) and sacrificed at different time periods (n = 2–5 mice/group). **(C)** *Il6* and *Tnfa* mRNA expression in BAT (n = 4 mice/group). (**D**) Western blotting and quantification showing levels of insulin-induced IR and AKT (Ser 473) phosphorylation after LPS and insulin injections (n = 5–6 mice/group). (**E**) Western blotting and quantification of UCP-1 protein expression in BAT from the mice receiving LPS or not and exposed to 4 °C for the last 6 h (n = 8–10 mice/group). The right panel shows UCP-1 immunohistochemistry images (n = 3 mice/group). (**F**) The graphs show skin temperature of the BAT area and rectal temperature (n = 7–17 mice/group). The middle panel shows representative images. (**G**) Nuclei quantification in different BAT sections (3–4 mice/group). The right panel shows representative H&E staining BAT images. Scale bars represent 50 μm. Data are expressed as mean ± SEM. Statistical analysis in **A**, **D**, and **E** was conducted with the Mann–Whitney U test. Statistical analysis in **B**, **C**, **F**, and **G** was performed by two-way ANOVA. *Comparisons between LPS-treated and untreated mice with the same genotype. #Comparison between genotypes receiving the same treatment. $^{*,\#}p < 0.05$, $^{**,\#\#}p < 0.01$, and $^{***}p < 0.001$.

 

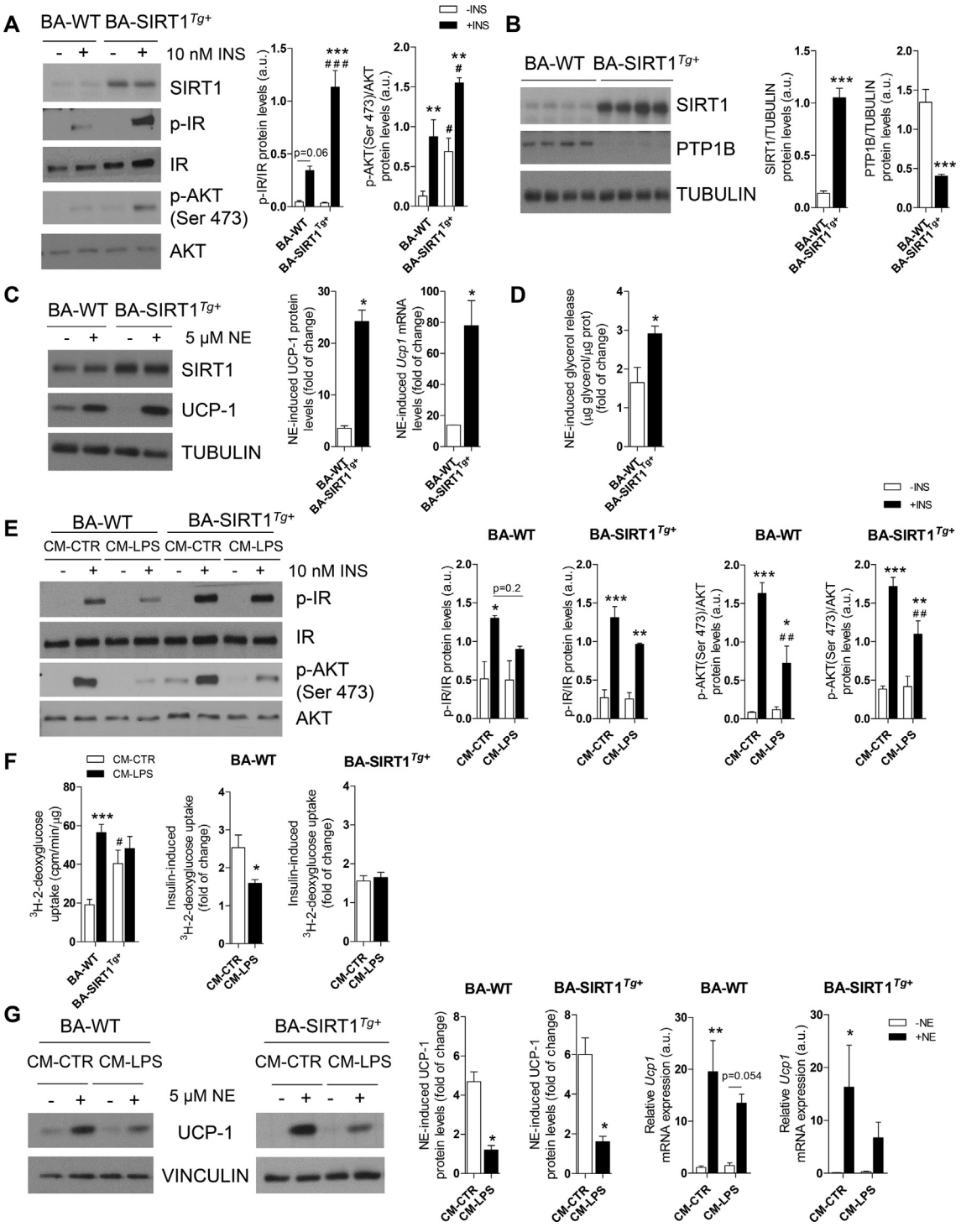


**Figure 3: SIRT1 overexpression conferred protection against insulin resistance, but not UCP-1 induction, in brown adipocytes under pro-inflammatory conditions. (A)** Western blotting and graphs showing IR and AKT phosphorylation in BA with or without insulin (n = 3–4 independent experiments). (**B**) Western blotting and quantification of PTP1B and SIRT1 (n = 7–8 independent experiments). (**C**) Western blotting and quantification of fold change of UCP-1 (protein and mRNA) after NE stimulation (n = 3–4 independent experiments). (**D**) Glycerol released after NE stimulation (n = 3 independent experiments). (**E**) Western blotting and quantification of insulin-induced IR and AKT phosphorylation after CM-CTR or CM-LPS treatment (n = 3–4 independent experiments). (**F**) The left graph represents the basal $^{3}$H-2-deoxyglucose uptake in BA (n = 4 independent experiments) and the right graphs represent the fold increase in insulin-induced glucose uptake after treatment with CM-CTR or CM-LPS for 18 h and further stimulated with insulin (10 nM) (n = 4 independent experiments). (**G**) Western blotting and graphs showing the fold increase in UCP-1 (protein and mRNA) after NE stimulation (n = 3–5 independent experiments). Results are expressed as mean ± SEM. The statistical analysis in **A**, **E**, **F** (left graph), and **G** (right graphs) was performed by two-way ANOVA. *Comparisons between treated and untreated BA with the same genotype. #Comparison between genotypes receiving the same treatment. Statistical analysis in **B-D** was conducted with Mann–Whitney U test. *Comparison between genotypes. Statistical analysis in **F** (right graph) and **G** (left graph) was performed with the Mann–Whitney U test. *Comparison between treatments. $^{*,\#}p < 0.05$, $^{**,\#\#}p < 0.01$, and $^{***,\#\#\#}p < 0.001$.

 

increased levels was observed in the SIRT1$^{Tg+}$ mice. At the protein level, histological and Western blotting analysis of UCP-1 showed a decrease in both genotypes with a slightly attenuated effect in the SIRT1$^{Tg+}$ mice (Figure S3C). Next, to address a possible effect of inflammation and/or SIRT1 overexpression on BAT respiration, a Seahorse analysis was conducted in BAT explants from the mice receiving LPS or not. A trend of higher basal and increased maximal respiration was found in the SIRT1$^{Tg+}$ mice (Figure S3D). Moreover, basal and maximal respiration decreased in BAT explants from the LPS-injected WT or SIRT1$^{Tg+}$ mice.

To further evaluate the impact of LPS-mediated inflammation and SIRT1 overexpression on BAT, we subjected the WT and SIRT1$^{Tg+}$ mice to the cold under pro-inflammatory conditions. The mice were housed at 28 °C for 1 week and then randomly divided into 2 experimental groups, one that was exposed to 4 °C for 6 h. The other group was injected with LPS and exposed to 4 °C for the last 6 h of a total of 24 h. Notably, no differences among genotypes were found in the induction of thermogenic-related genes upon cold exposure (Figure S4A). The UCP-1 protein levels decreased in BAT from the WT mice injected with LPS and exposed to 4 °C; this effect was ameliorated in the SIRT1$^{Tg+}$ mice (Figure 2E). At the mRNA level, *Prdm16* and *Dio2* expression significantly decreased after LPS injection plus cold exposure compared to the cold exposure condition exclusively in the WT mice (Figure S4B). In line with these data, the rectal and skin BAT area temperatures significantly decreased in the WT animals after exposure to LPS and cold compared to the SIRT1$^{Tg+}$ mice (Figure 2F). In addition, in the SIRT1$^{Tg+}$ mice, the BAT and iWAT weight was lower after LPS injection and cold exposure compared to the WT animals (Figure S4C). When analyzing BAT histology, fewer nuclei per field were counted in the WT mice subjected to LPS and cold, an effect not observed in the SIRT1$^{Tg+}$ mice (Figure 2G). Overall, these evidences suggested that LPS promoted impairment of BAT thermogenic capacity as well as protection by moderate SIRT1 overexpression.

### 3.3. Moderate SIRT1 overexpression blunted inflammation-induced impairment in insulin and adrenergic responses in brown adipocytes

We used immortalized brown preadipocytes to identify the molecular mechanisms related to the protective effects against inflammation shown by the SIRT1$^{Tg+}$ mice. In agreement with our previous study [36], terminally differentiated BA from the SIRT1$^{Tg+}$ mice (called BA-SIRT1$^{Tg+}$) had lower *Ucp1* mRNA and UCP-1 protein levels than BA-WT (Figure S5A). No differences between genotypes were detected in the protein levels of adipogenic markers such as fatty acid synthase (FAS) or relevant insulin signaling proteins (IR and GLUT4). We next evaluated cell autonomous insulin signaling in BA and our data revealed higher insulin-stimulated IR and AKT phosphorylation in BA-SIRT1$^{Tg+}$ (Figure 3A). Notably, these cells showed higher basal AKT phosphorylation in the absence of insulin. Also, as reported by Sun *et al.* in skeletal muscle cells [39], moderate SIRT1 overexpression concurred with the downregulation of protein tyrosine phosphatase 1B (PTP1B) protein levels in BA (Figure 3B). The impact of moderate SIRT1 overexpression in the response to norepinephrine (NE) was also evaluated. BA-SIRT1$^{Tg+}$ showed a higher NE-induced response on UCP-1 compared with BA-WT (Figure 3C). Moreover, NE-induced lipolysis as measured by glycerol release to the culture medium was also higher in BA overexpressing SIRT1 (Figure 3D).

Local proliferation of macrophages in adipose tissues contributes to inflammation during obesity [51]. To analyze the cross-talk between macrophages and the BA responses, conditioned medium (CM) was collected from Raw 267.4 macrophages stimulated or not with LPS (called CM-LPS and CM-CTR, respectively) and the pro-inflammatory potency of CM-LPS was assessed by quantifying nitrite production (Figure S5B). To analyze the effect of CM-LPS on the activation of pro-inflammatory signaling cascades, differentiated BA from both genotypes was treated with either CM for different time periods ranging from 15 to 120 min. As expected, in BA-WT, the exposure to CM-LPS triggered an early activation of the signaling pathways mediated by STAT3, IKK$\alpha/\beta$, JNK, and p38 MAPK (Figure S5C). Interestingly, BA-SIRT1$^{Tg+}$ showed a significant decrease in STAT3 phosphorylation compared to BA-WT at all of the time periods analyzed.

We next evaluated the responses of BA to insulin or NE in the presence of pro-inflammatory CM-LPS. Treatment with CM-LPS decreased insulin-mediated IR and AKT phosphorylation in BA-WT compared with the response in the presence of CM-CTR (Figure 3E). However, this effect was ameliorated in BA-SIRT1$^{Tg+}$. Since BAT is a glucose-clearing organ [52], the effect of the pro-inflammatory environment on glucose uptake was measured in BA. We observed an increase in basal (insulin-independent) glucose uptake in BA-WT after the treatment with CM-LPS that was absent in BA-SIRT1$^{Tg+}$. Notably, BA overexpressing SIRT1 showed higher basal levels of glucose uptake under non-pro-inflammatory conditions (CM-CTR) that did not further increase in the presence of CM-LPS (Figure 3F). The analysis of the insulin response revealed a marked reduction in glucose uptake in BA-WT pre-treated with CM-LPS that did not occur in BA-SIRT1$^{Tg+}$. In the same line, the response of BA to NE in the presence of CM-LPS evidenced a decrease in UCP-1 protein levels in BA-WT (Figure 3G). Unexpectedly, SIRT1 overexpression failed to protect against the decrease in UCP-1 protein content, although his reduction was less evident at the mRNA level.

### 3.4. Differentiation of brown adipocytes in medium enriched in $T_3$, insulin, and rosiglitazone enhanced their thermogenic program

To overcome the failure of BA-WT and BA-SIRT1$^{Tg+}$ to respond to NE under pro-inflammatory conditions, preadipocytes were differentiated using a protocol previously used by Quesada-López *et al.* to differentiate subcutaneous white adipocytes into beige adipocytes [44], but not previously used to differentiate BA. This differentiation medium (called medium 2) is enriched in $T_3$, rosiglitazone, and insulin compared to the medium broadly used to differentiate brown preadipocytes (called medium 1; see Materials and Methods). Although the differentiation of preadipocytes from both genotypes with either medium was comparable (Figure 4A, left panel), staining of lipid droplets with Bodipy revealed higher lipid accumulation in BA differentiated with medium 2 (Figure 4A, right panel). Interestingly, *Dio2* mRNA levels were downregulated in both BA genotypes differentiated in medium 2 compared to medium 1 (Figure 4B), probably due to elevated $T_3$ concentrations [53]. BA-WT differentiated with medium 2 showed a marked increase in *Prdm1*6 mRNA levels compared with the levels found in these cells upon differentiation with medium 1. Importantly, *Prdm16* expression was elevated regardless of the differentiation medium in BA-SIRT1$^{Tg+}$. Moreover, both BA-WT and BA-SIRT1$^{Tg+}$ showed much higher *Ucp1* mRNA and UCP-1 protein levels at the final stage of differentiation with medium 2 compared to medium 1 (Figure 4B). However, no differences in *Pgc1a* mRNA levels were found regardless of the genotype or differentiation medium.

We next investigated if medium 2 could affect the metabolism of BA. Metabolomic analysis revealed an increase in metabolites of the tricarboxylic acid cycle (TCA) such as $\alpha$-ketoglutarate, succinate, and glutamic acid but not glutamine compared to the levels detected in both BA genotypes differentiated with medium 1 (Figure 4C). Moreover, an increase in ribose and gluconic acid lactone, intermediates of the phosphate pentose cycle (PPC), was found in BA differentiated with

 

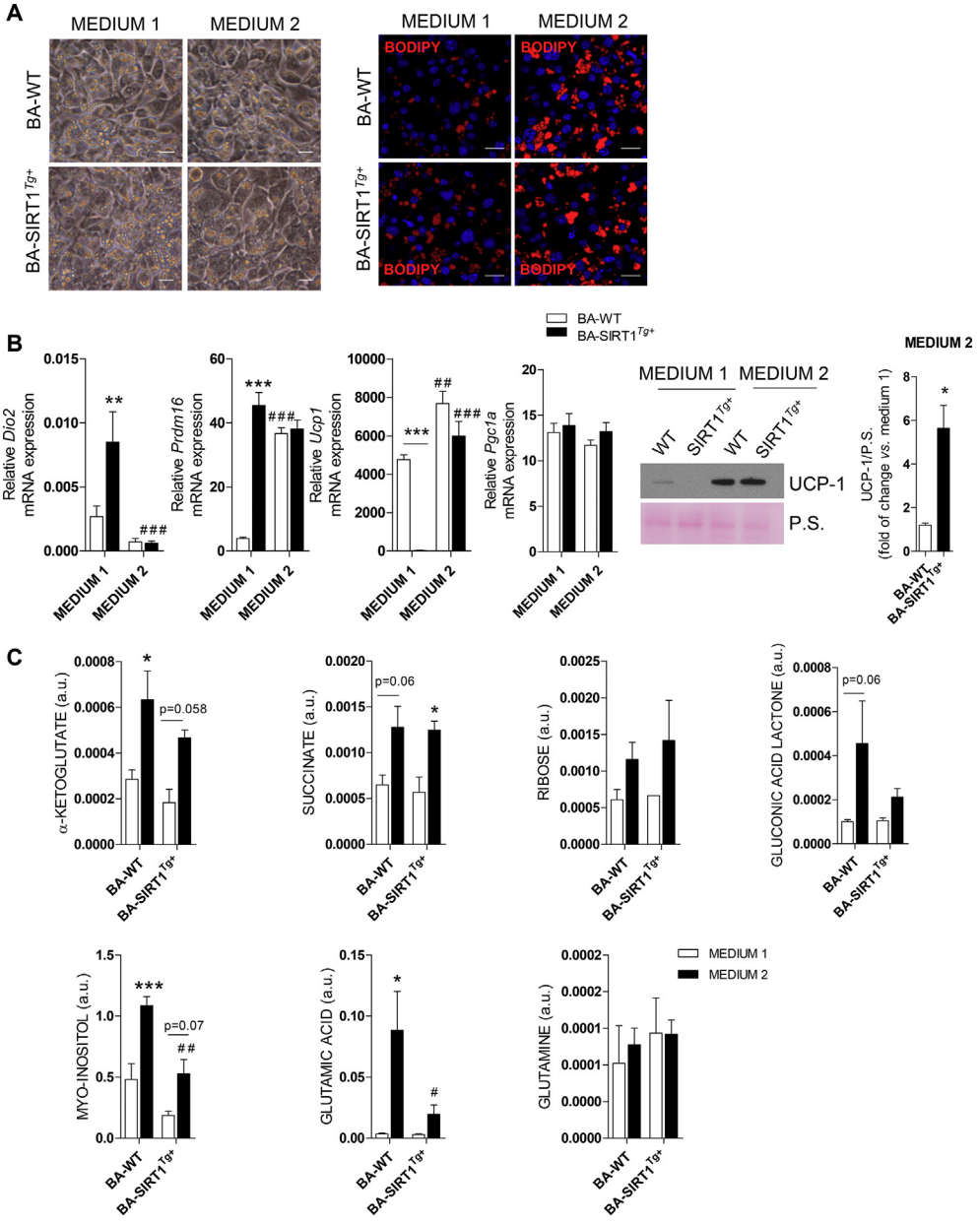


**Figure 4: Differentiation of BA from the WT and SIRT1$^{Tg+}$ mice with $T_3$, insulin, and rosiglitazone-enriched medium impacted the metabolic and thermogenic profiles.** (**A**) Microscopy images and Bodipy immunofluorescence (red) in BA differentiated with medium 1 or 2. Scale bars represent 20 μm. (**B**) (left) *Dio2*, *Ucp1*, *Prdm16*, and *Pgc1a* mRNA levels in BA on day 7 of differentiation with the two media analyzed by qRT-PCR relative to levels on day 0 ($n = 5–6$ independent experiments). (right) Representative Western blotting and quantification of UCP-1 protein levels on days 0 and 7 of differentiation of BA with medium 1 or 2 ($n = 4$ independent experiments). (**C**) Metabolomic analysis in BA differentiated with medium 1 or 2 (day 7) ($n = 2–3$ independent experiments). Results are expressed as mean ± SEM. Statistical analysis in **B** (right) was performed with Mann–Whitney U test. *Comparison between genotypes. The statistical analysis in **B** (left) and **C** was conducted by two-way ANOVA. (**B**) (left) *Comparison between different genotypes and the same medium. #Comparison between the two media and the same genotype. (**C**) *Comparison between the same genotype and different media. #Comparison between genotypes differentiated with the same medium. $^{*,\#}p < 0.05$, $^{**,\#\#}p < 0.01$, and $^{***,\#\#\#}p < 0.001$. P.S., Ponceau staining.

medium 2. Likewise, the antioxidant metabolite myo-inositol was also increased. These results demonstrate an effect of medium 2 on the metabolic profile of differentiated BA in a SIRT1-independent manner. We also addressed a possible effect of medium 2 in the amount of mitochondria in BA by performing TOM 22 and COX-IV immunofluorescence. A higher signal of both markers was detected in BA overexpressing SIRT1 (Figure S6A). Mitochondrial mass was also measured by flow cytometry using MitoTracker Green. Although BA-SIRT1$^{Tg+}$ showed significantly higher mitochondrial mass compared to BA-WT upon differentiation with medium 1, medium 2 led to differentiated BA of the two genotypes with less mitochondrial mass. Mitochondrial dynamics was also studied in BA on day 7 with either differentiation medium by immunofluorescence and Western blotting of phosphorylated DRP1 (p-DRP1) and mitofusin 2 (MFN2) as markers of mitochondrial fission and fusion, respectively. Our results showed higher p-DRP1 levels in BA-WT and BA-SIRT1$^{Tg+}$ differentiated with medium 2 while MFN2 decreased (Figure S6B), demonstrating similar changes in mitochondrial dynamics.

 

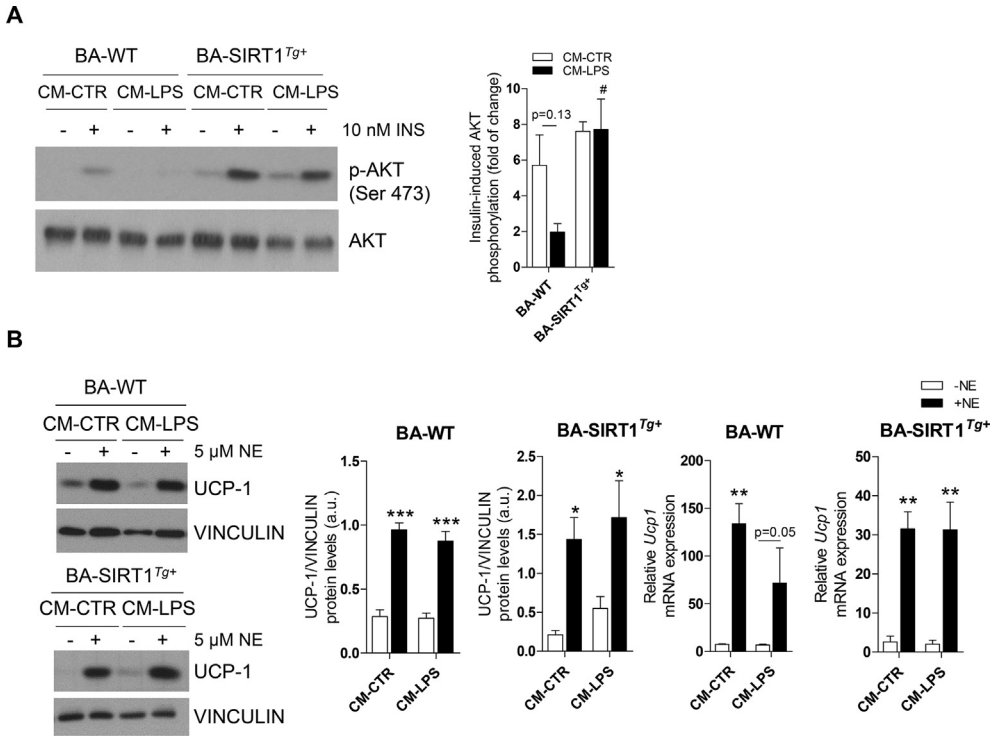


**Figure 5: Differentiation of brown adipocytes in medium enriched in $T_3$, insulin, and rosiglitazone conferred protection against inflammation in insulin and noradrenergic responses.** (**A**) Western blotting and quantification of insulin-induced AKT phosphorylation (n = 3 independent experiments). (**B**) Western blotting and quantification of UCP-1 (n = 4 independent experiments) and *Ucp1* mRNA levels (n = 2–3 independent experiments) after differentiation of BA with medium 2 and treatment with CM-CTR or CM-LPS in the absence or presence of NE. Results are expressed as mean ± SEM. Statistical analysis was performed by two-way ANOVA. (**A**) $^{\#}$Comparison between genotypes with the same treatment. (**B**) $^{*}$Comparisons between NE-treated and untreated BA with the same genotype. Bars represent mean ± SEM. $^{*,\#}p < 0.05$, $^{**}p < 0.01$, and $^{***}p < 0.001$.

To study the responses to insulin or NE in BA differentiated with medium 2, we analyzed insulin signaling as well as UCP-1 protein and its mRNA levels after the same treatments described for medium 1 (Figure 3A,B, and C). Data on insulin signaling showed higher basal IR and AKT phosphorylation in BA-SIRT1$^{Tg+}$ and a marked tendency to increase in their response to insulin (Figure S6C). Of note, as occurred in the cells differentiated in medium 1 (Figure 3B), the PTP1B protein levels remained downregulated in BA-SIRT1$^{Tg+}$ differentiated with medium 2 (Figure S6D). Medium 2 also led to higher *Ucp1* mRNA levels in NE-treated BA-WT or BA-SIRT1$^{Tg+}$ (Figure 6E); this effect was even enhanced by SIRT1 overexpression. Regarding UCP-1 protein levels, an increased response to NE was detected in BA-SIRT1$^{Tg+}$ differentiated with medium 2, an effect due in part to reduced basal levels. Likewise, BA-SIRT1$^{Tg+}$ showed a higher NE-induced lipolytic rate compared to the response of BA-WT (Figure S6E). Comparison between the effect of NE in increasing *Ucp1* mRNA levels in BA differentiated with each medium revealed a fourfold increase in both BA genotypes differentiated with medium 2 (Figure S6F).

Taking into account the relationship between $T_3$ and SIRT1 [24], we hypothesized that medium 2 might modulate SIRT1 activity. The analysis of p65-NFκB acetylation as a readout revealed a decrease in BA-WT differentiated with medium 2 (Figure S7A). As expected, SIRT1 overexpression decreased acetylation of p65-NFκB in BA differentiated with either medium 1 or 2. Lower ATP levels were detected in both genotypes after differentiation with medium 2 (Figure S7B). This decrease in ATP levels could be indicative of higher SIRT1 activity as previously reported [54]. In agreement, BA-SIRT1$^{Tg+}$ showed lower ATP levels than those of BA-WT regardless of the differentiation medium used. We next addressed whether inflammation could modulate ATP levels in BA. For this purpose BA were stimulated with CM-CTR or CM-LPS. Treatment with CM-LPS decreased ATP levels in BA-WT differentiated with either medium 1 or 2. In contrast, ATP levels did not further decrease in BA-SIRT1$^{Tg+}$ differentiated with medium 2 (Figure S7C).

### 3.5. Differentiation of brown adipocytes in medium enriched in $T_3$, insulin, and rosiglitazone conferred protection against pro-inflammatory conditions

We investigated whether medium 2 would confer protection against the activation of pro-inflammatory signaling cascades and subsequent reduction in insulin and noradrenergic responses induced by CM-LPS. This analysis revealed lower activation of STAT3 in BA-WT differentiated with medium 2 with respect to the response in medium 1 (Figure S8A) and moderately less activation of the inflammatory cascades in BA-SIRT1$^{Tg+}$ (Figure S8B). In the same line of the results obtained with medium 1 (Figure 3A,3E), moderate SIRT1 overexpression enhanced insulin-mediated AKT phosphorylation and protected against the decrease in this response in the presence of pro-inflammatory CM-LPS (Figure 5A). We also assessed whether differentiation of BA with medium 2 could prevent the decline in NE-induced UCP-1 activation under pro-inflammatory conditions. Contrary to the results depicted in Figure 3G, both BA genotypes differentiated in medium 2 increased UCP-1 protein and *Ucp1* mRNA levels in response to NE in the presence of CM-LPS (Figure 5B).

Seahorse analysis was conducted to study more in-depth mitochondrial respiration capacity of BA upon differentiation with either

 

medium 1 or 2 and treatment with pro-inflammatory CM-LPS. Fatty acid oxidation (FAO) was also measured to evaluate their oxidative capacity. The Seahorse profile revealed no impact of the pro-inflammatory environment on the complexes of the electron transport chain (ETC) in BA differentiated with medium 1 (Figure 6A). Likewise, no differences were found in the effect of oligomycin, FCCP, or rotenone/antimycin A. Regarding FAO analyzed by detecting $CO_2$ and acid-soluble products (ASPs) released from oxidation of palmitate, BA-SIRT1$^{Tg+}$ showed higher basal levels that decreased after treatment with CM-LPS but remained higher than those of BA-WT. Similar research was conducted in BA differentiated with medium 2 and the Seahorse profile revealed increased basal OCR compared to medium 1 (Figure 6A,B). Moreover, increased OCR was also found in BA-WT differentiated with medium 2 after treatment with CM-LPS (blue lines in Figure 6B). However, we did not find differences in the impact of the pro-inflammatory environment on OCR levels in BA-SIRT1$^{Tg+}$ (purple and pink lines). In addition, FAO analysis revealed an increase in $CO_2$ and ASPs released from palmitate oxidation in BA-SIRT1$^{Tg+}$ after treatment with CM-CTR or CM-LPS compared to the BA-WT levels (Figure 6B). Moreover, the metabolomic analysis in BA differentiated with medium 2 showed a marked increase in α-ketoglutarate and succinate, both TCA metabolites related to anti-inflammatory responses in macrophages [55,56] and glycerol as well as a tendency to increase in glutamine in BA-SIRT1$^{Tg+}$ after exposure to CM-LPS (Figure 6C). However, these effects were absent in BA-WT.

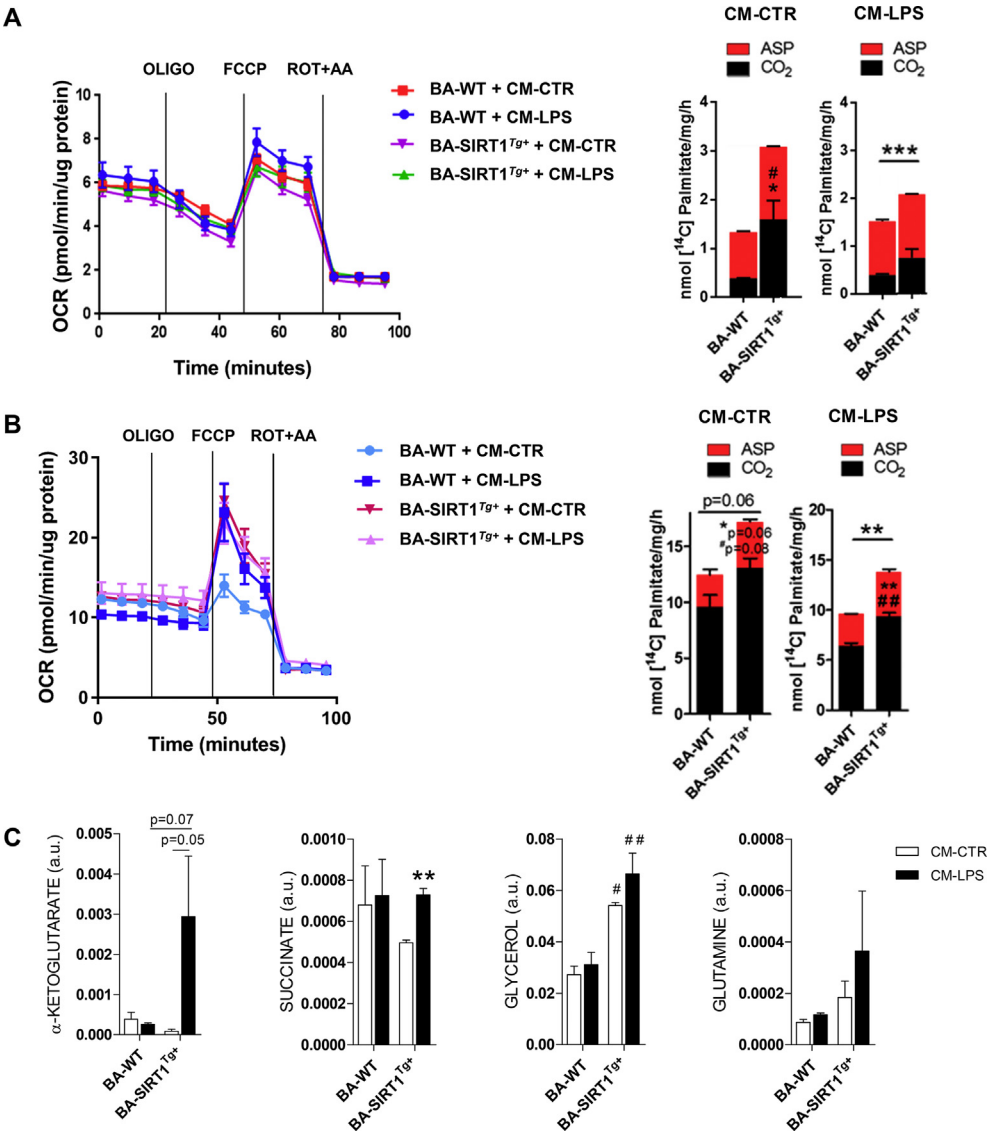


**Figure 6: A pro-inflammatory environment impacted the Seahorse, metabolic profiles, and noradrenergic response of BA-WT and BA-SIRT1$^{Tg+}$ differentiated with $T_3$, insulin, and rosiglitazone-enriched medium.** (**A**) Seahorse profile and FAO assay in BA differentiated with medium 1 treated with CM-CTR or CM-LPS for 18 h (n = 3 independent experiments). (**B**) Seahorse profile (one experiment performed in quintupled) and FAO assay (n = 3 independent experiments) in BA differentiated with medium 2 and treated with CM-CTR or CM-LPS for 18 h. (**C**) Metabolomic analysis in BA differentiated with medium 2 and treated with CM-CTR or CM-LPS for 18 h (n = 2–3 independent experiments). In **A** and **B**, statistical analysis was conducted with the Mann–Whitney U test. *Comparison of ASPs between genotypes. #Comparison of $CO_2$ levels between genotypes. In **C**, the statistical analysis was performed by two-way ANOVA. *Comparison between CM-LPS and CM-CTR-treated BA differentiated in same genotype. #Comparison between genotypes with the same treatment. *Comparison between genotypes. Bars represent mean ± SEM. $^{*,\#}p < 0.05$, $^{**,\#\#}p < 0.01$, and $^{***}p < 0.001$.

 

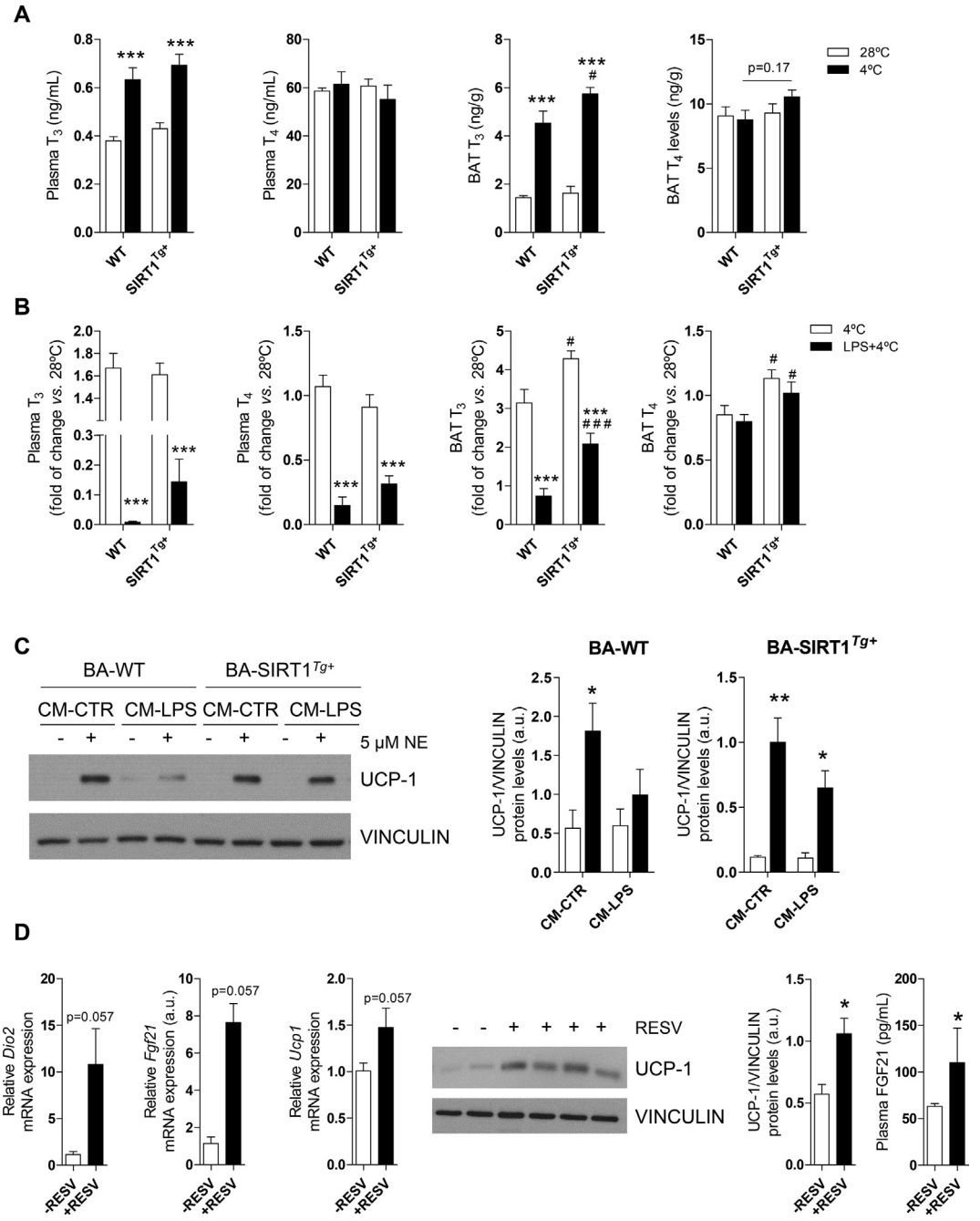


**Figure 7: Differences in plasma and BAT THs levels in the WT and SIRT1$^{Tg+}$ mice after inflammation and cold exposure. Effect of resveratrol in BAT from the *db/db* mice.** (**A**) $T_3$ and $T_4$ levels in plasma and BAT at thermoneutrality or after cold exposure (n = 5–10 mice/group). **(B)** Fold change of $T_3$ and $T_4$ levels in plasma and BAT after cold exposure of LPS-injected or non-injected mice (n = 7–13 mice/group). Data are referred to the WT group maintained at 28 °C. **(C)** Western blotting and quantification of UCP-1 levels in BA differentiated in medium 1 supplemented with $T_3$ (n = 3 independent experiments) **(D)** (left) Graphs show *Dio2*, *Fgf21*, and *Ucp1* mRNA levels in BAT (n = 3–4 mice/group) from the *db/db* mice treated with resveratrol. (middle) Representative western blotting showing UCP-1 levels in BAT and quantification (n = 3–4 mice/group). (right) Circulating FGF21 levels. Results are expressed as mean ± SEM. The statistical analysis in **A-B** was performed with two-way ANOVA. *Comparison between the mice at 28 °C and 4 °C or between the LPS-injected or non-injected mice. #Comparison between the same conditions and different genotypes. In **C**, statistical analysis was conducted with two-way ANOVA. *Comparison between CM-LPS and CM-CTR-treated BA differentiated in the same genotype. In **D**, statistical analysis was performed with the Mann–Whitney U test. $^{*,\#}p < 0.05$, $^{**}p < 0.01$, and $^{***,\#\#\#}p < 0.001$.

### 3.6. $T_3$ and $T_4$ in plasma and BAT were modulated in SIRT1$^{Tg+}$ mice exposed to LPS and cold

As the *in vitro* data established a direct relationship between differentiation of BA in the presence of high $T_3$ levels and increased UCP-1 under normal or pro-inflammatory conditions, we analyzed $T_3$ and $T_4$ levels in plasma and BAT from the WT and SIRT1$^{Tg+}$ mice exposed to both pro-inflammatory and thermogenic conditions. The WT and SIRT1$^{Tg+}$ mice showed increased $T_3$ levels in their circulation and BAT upon cold exposure; the abundance of intra-BAT $T_3$ was higher in the SIRT1$^{Tg+}$ mice challenged with cold (Figure 7A). However, after

 

injection of LPS before cold exposure, the SIRT1$^{Tg+}$ mice exhibited a trend (non-significant) of less decrease in $T_3$ plasma levels compared to the WT mice and significant protection against the decrease in intra-BAT $T_3$ content (Figure 7B). The combination of LPS injection and cold exposure equally decreased circulating $T_4$ in both mouse genotypes and did not affect the intra-BAT content of $T_4$ although the SIRT1$^{Tg+}$ mice had higher levels. The relationship between SIRT1 and $T_3$ was also tested in BA differentiated with medium 1 and supplemented with only $T_3$ up to a similar concentration as in medium 2. As shown in Figure 7C, under this condition, BA-SIRT1$^{Tg+}$ were more sensitive to NE in the presence of CM-LPS compared to BA-WT.

### 3.7. Resveratrol increased *Dio2* mRNA levels and UCP-1 expression in BAT in the *db/db* mice

To enhance UCP-1 protein in BAT using a pharmacological approach targeting THs and SIRT, we treated the *db/db* mice with SIRT1 activator resveratrol. Treatment of the *db/db* mice with resveratrol for 8 weeks decreased their blood glucose without changes in body weight (Figure S1F,S1G). Interestingly, increased *Dio2* and *Fgf21* mRNA levels, the latter recently associated by Villarroya *et al.* with increases in UCP-1 [15], were found in BAT from the resveratrol-treated *db/db* mice in parallel with elevations in circulating FGF21 and increased UCP-1 expression in the mRNA and protein levels in BAT (Figure 7D).

## 4. DISCUSSION

Pro-inflammatory signals have recently been recognized as potential negative modulators of BAT functionality. The results presented herein evidenced inflammatory features in BAT from the *db/db* mice manifested by enhanced pro-inflammatory signaling and gene expression in this fat depot, an effect that correlated with tissue-specific insulin resistance as reported in other organs [57—60]. Of relevance, as occurred in the muscle or liver in insulin-resistant states [61,62], an altered IRA/IRB ratio was found in BAT from the *db/db* mice with a robust IRA presence that could account, at least in part, for the impaired insulin signaling, an effect likely due to metabolic immaturity of this tissue. Whether the unbalanced IRA/IRB ratio in BAT from the *db/db* mice was a direct consequence of systemic and/or local inflammation deserves future research.

Seeking a causative factor for the onset of inflammation-mediated insulin resistance in BAT, we explored whether endotoxemia was sufficient to trigger pro-inflammatory signaling cascades in this tissue. Based on previous studies [63,64], we injected a non-septic dose of LPS into the WT mice and found a pro-inflammatory signaling signature in BAT similar to that of the *db/db* mice. Of note, these pathways negatively impact insulin signaling at different levels [65—67] and are likely responsible for the impairment of IR and AKT phosphorylation in BAT from the LPS-injected or *db/db* mice.

Several studies have reported a role of SIRT1 in the protection against metabolic damage linked to obesity [33,34,36] and its benefit in alleviating LPS-induced metabolic dysfunction in lung [68], keratinocyte [69], or endothelial cells [70]. Our study provides previously unknown evidence of the protection against the decline in IR and AKT phosphorylation in BAT from LPS-injected SIRT1$^{Tg+}$ mice in line with the recently reported alleviation of fatty liver by SIRT1 activation [71]. The *in vitro* studies in BA with moderate SIRT1 overexpression showed increased insulin-induced IR and AKT phosphorylation compared to BA-WT in parallel with reduced PTP1B protein levels. This agrees with the work of Sun *et al.* on improving insulin sensitivity in hepatocytes and myotubes by enhancing SIRT1 expression/activity through repression of PTP1B [39]. A step further and to verify the protective effect of moderate SIRT1 overexpression in BA in an inflammatory context, we conducted cell-based experiments mimicking their cross-talk with macrophages. The decrease in STAT3 phosphorylation in BA-SIRT1$^{Tg+}$ treated with pro-inflammatory CM-LPS suggests specific modulation of the JAK-STAT pathway by SIRT1 in BA [72]. Furthermore, BA-SIRT1$^{Tg+}$ were protected against the decline in insulin-mediated IR and AKT phosphorylation under pro-inflammatory conditions compared to BA-WT, probably by synergy of lower PTP1B and less STAT3 phosphorylation, the latter described in 3T3L1 adipocytes demonstrating a relationship between SOCS3, STAT3, and insulin signaling in adipose cells [73—75]. Of relevance, in both WT and SIRT1 overexpressing BA, the impact of the pro-inflammatory CM was higher in the AKT phosphorylation response. This was likely due to alternative mechanisms triggered by pro-inflammatory cytokines such as increased SOCS3 [75], which impairs insulin receptor substrate-1-mediated signaling downstream IR and upstream AKT. Of note, the inflammatory CM-LPS upregulated basal (insulin-independent) glucose uptake in BA-WT, thereby ameliorating the effect of insulin as occurred in myotubes and white adipocytes treated with TNF$\alpha$, IL-1$\beta$, or IL-6 [76—78], an effect probably mediated by the upregulation of GLUT-1 [79]. Moreover, the pro-inflammatory CM-LPS led to a decrease in insulin-induced glucose uptake in BA-WT as found in other insulin-sensitive cells including white adipocytes [80] that might be related to the decrease in AKT phosphorylation [81]. In contrast, in BA-SIRT1$^{Tg,+}$ CM-LPS did not increase insulin-independent glucose uptake or decrease insulin-mediated glucose uptake under pro-inflammatory conditions and preserved the threshold AKT phosphorylation levels. Our results agree with Yoshizaki *et al.*, showing that SIRT1 activators increased glucose uptake and insulin signaling in white adipocytes and rescued from TNF-$\alpha$-induced insulin resistance [82]. Likewise, Chen *et al.* described that SIRT1 activation by resveratrol increased glucose uptake in insulin-resistant 3T3-L1 adipocytes [83].

Although evidence of the involvement of SIRT1 in increasing energy expenditure has been reported [33,34,36], the impact of its moderate overexpression/activation in BAT thermogenesis under a pro-inflammatory context has not been explored. Of note, SIRT1 overexpression was associated with enhanced energy expenditure and transcriptional responses to $\beta$-adrenergic stimulation in BAT [33,36,84—86]. In agreement with those previous studies, herein we showed elevations in the temperature of the skin BAT area, as well as in basal and maximal respiration, in BAT explants from the SIRT1$^{Tg+}$ mice in parallel with higher UCP-1 protein and mRNA levels. Interestingly, histological evaluation revealed lipid-depleted BAT sections in the mice with moderate overexpression of SIRT1, a feature of tissue activation. This BAT morphology likely resulted from the increased basal lipolytic rate as we previously reported [36]. However, after exposing the mice to thermoneutrality followed by cold challenge, we did not detect differences in thermogenic-related genes among the mice without or with moderate SIRT1 overexpression. These data differ from those of Gerhart-Hines *et al.* that found increased basal and cold-induced *Ucp1* mRNA in BAT from SirBACO mice [84]. A potential explanation for such differences can be attributed to different mice strains and the absence of thermoneutral conditions before cold exposure in their study. Regarding the impact of inflammation in BAT independent of obesity, Nohr *et al.* reported reduced expression of brown-related genes in mice chronically infused LPS, an effect associated with a switch in polarization of BAT resident macrophages to the M1 state [87]. A step further, our results in mice exposed to LPS and cold revealed that moderate SIRT1 overexpression protected against decreases in rectal temperature, skin BAT area temperature,

 

and the decline in UCP-1 protein levels. In addition, histology of the BAT sections showed a further decrease in the lipid content in the SIRT1$^{Tg+}$ mice, suggesting a more effective utilization of lipids stored in BAT droplets as thermogenic fuel to maintain body temperature.

To obtain further insight into the cell-autonomous effects of moderate SIRT1 overexpression, we studied the response of BA-WT and BA-SIRT1$^{Tg+}$ to NE. Previous results showed that terminally differentiated BA from SIRT1$^{Tg+}$ mice expressed less UCP-1 under basal conditions [36], in line with the role of SIRT1 as a metabolic sensor triggering adaptations to optimize energy production [88]. In contrast and in agreement with this previous study, BA-SIRT1$^{Tg+}$ showed higher *Ucp1* mRNA and protein levels upon β-adrenergic stimulation, demonstrating their better responsiveness upon a thermogenic stimulus. Of relevance, the results presented herein revealed that *Ucp1* mRNA and protein levels decreased in BA-WT exposed to CM-LPS and NE as pro-inflammatory and β-adrenergic stimuli, respectively. In this line, the suppression of isoproterenol-induced UCP-1 activation by macrophage-derived CM was reported in 10T1/2 adipocytes derived from mouse mesenchymal stem cells [89]. However, we found an unexpected response in BA-SIRT1$^{Tg+}$ in which the pro-inflammatory milieu impaired their response to NE in inducing UCP-1 as in BA-WT. Of note, the expression or activity of SIRT1 were attenuated by LPS in endothelial cells [70], Kupffer cells [90], and Raw 264.7 macrophages [90–92]. Therefore, the failure of moderate SIRT1 overexpression to counteract the decline in UCP-1 in BA in a pro-inflammatory environment might be due to a decrease in SIRT1 activity under this condition. Of note, the different results found in BA vs BAT from the SIRT1$^{Tg+}$ mice regarding the protection against the decline in UCP-1 under pro-inflammatory conditions could have been due to the anti-inflammatory effect of cold-induced M2 polarized resident macrophages in BAT tissue [93] that might have counteracted LPS-induced inflammation.

To find an alternative protocol to differentiate brown preadipocytes to mature cells resistant to the deleterious effects of CM-LPS, we adapted a method used for inducing "browning" of inguinal white adipocytes [44]. This medium (called medium 2) was enriched in insulin, rosiglitazone, and $T_3$, all major triggers of BAT adipogenic and thermogenic programs [2,94,95]. $T_3$ is classically considered a stabilizer of *Ucp1* mRNA levels [17,18] as evidenced by increased *Ucp1* mRNA and UCP-1 protein levels upon differentiation of BA with medium 2. This effect was not related to changes in *Pgc1a* and was markedly enhanced in BA-SIRT1$^{Tg+}$ that presented very low UCP-1 protein levels upon differentiation in medium 1 as previously mentioned. A possible factor contributing to the increased UCP-1 levels in terminally differentiated BA in medium 2 could have been related to a switch in mitochondrial dynamics revealing, on the one hand, lower fusion (MFN2) in parallel with less ATP levels as reviewed by Lee *et al.* [96] and, on the other hand, higher p-DRP1, a readout of fission, in agreement with elevated p-DRP1 reported in activated BAT and also with reduced uncoupled respiration in BA by the blockade of mitochondrial fission [97,98].

$T_3$ increases intracellular $NAD^+$/NADH and activates SIRT1 in both hepatocytes and BA [24] and also increases SIRT1 expression and activity in livers of rats treated with rosiglitazone [99]. Therefore, we demonstrated higher SIRT1 activation monitored by reduced p65-NFκB acetylation in BA differentiated with medium 2. However, we could not distinguish if BA-SIRT1$^{Tg+}$ differentiated in medium 2 displayed higher SIRT1 enzymatic activity compared with BA-WT or BA-SIRT1$^{Tg+}$ differentiated in medium 1. Because commercially available tools to measure SIRT1 enzymatic activity have limited sensitivity, we indirectly addressed this issue by measuring ATP levels since Kang *et al.* demonstrated suppression of SIRT1 enzymatic activity by ATP [54]. In this regard, BA differentiated with medium 2 showed a substantial decrease in ATP levels; this effect was more pronounced in BA-SIRT1$^{Tg+}$. Of interest was the increase in *Prdm16* mRNA levels in BA-WT differentiated with medium 2. Ohno *et al.* suggested that the "browning" effect of PPAR ligands, including rosiglitazone, is due to stabilization of PRDM16 protein [100]. Taking into account this study, rosiglitazone *per se* and its effects mediated by PRDM16 likely contributed to enhanced UCP-1 levels in BA-WT differentiated with medium 2. Interestingly, as will be discussed, the supplementation of medium 1 with $T_3$ was sufficient to confer protection against the decline in UCP-1 by CM-LPS only in BA-SIRT1$^{Tg+}$ that already showed higher *Prdm16* mRNA levels upon differentiation with medium 1 compared to BA-WT. Medium 2 also contained a high concentration of insulin that in adipocytes favors fatty acid storage as triacylglycerol species in lipid droplets [101], an effect exacerbated in both BA genotypes differentiated under this condition. A metabolomic analysis was conducted to further explore differences in terminally differentiated BA with either medium. We detected an increase in α-ketoglutarate and succinate, two key TCA metabolites previously related to the suppression of IKKβ activation [55] or promotion of M2 polarization in macrophages [56], respectively, in BA differentiated with medium 2. The accumulation of succinate increased succinate dehydrogenase activity, resulting in the generation of reactive oxygen species that increased UCP-1 expression [102] and, in this line, we observed a direct relationship between the increase in succinate and UCP-1 in both BA genotypes differentiated in this medium. In fact, the elevation of these two intermediary TCA metabolites (succinate and α-ketoglutarate) could cooperate with the increased β-oxidation found in BA differentiated with medium 2, particularly in BA-SIRT1$^{Tg+}$, that showed a higher β-oxidation rate under basal conditions or in the presence of CM-LPS. Notably, α-ketoglutarate acts as a metabolic regulator that can also increase FAO [55]. Moreover, the anabolic PPC generates NADPH necessary for the lipogenic program and confers antioxidant properties. In this regard, we detected higher levels of ribose and gluconic acid lactone after differentiation of both BA genotypes with medium 2. In the same line, myo-inositol, a metabolite with direct antioxidant activity [103], also increased. Of interest is the increase in glycerol after LPS treatment in BA-SIRT1$^{Tg+}$ differentiated with medium 2 compared to BA-WT. This metabolite could be derived from the hydrolysis of triglycerides contained in BA lipid droplets generating FFAs as thermogenic fuel. Altogether, the results of the metabolomic analysis demonstrate the benefit of medium 2 in yielding differentiated BA with an anti-inflammatory metabolic signature.

Regarding insulin signaling and glucose uptake in a pro-inflammatory context, the results did not differ from medium 1, including the downregulation of PTP1B in BA-SIRT1$^{Tg+}$ and the rescue from insulin resistance. Conversely, both BA genotypes preserved the response to NE under pro-inflammatory conditions in increasing UCP-1 levels in medium 2 but, as previously mentioned, the enrichment in only $T_3$ was sufficient to rescue BA-SIRT1$^{Tg+}$, highlighting the cooperation of $T_3$ and SIRT1. It was previously suggested that in addition to the direct effects in BAT, THs also act indirectly via hypothalamic stimulation of sympathetic innervation, revealing a central role of $T_3$ in the hypothalamus-BAT axis by inducing lipolysis and mitochondrial uncoupling [104,105]. In agreement, we observed higher lipolysis in the two BA genotypes differentiated with medium 2 and, importantly, this response was more pronounced in BA-SIRT1$^{Tg+}$. In line with this, BAT from the SIRT1$^{Tg+}$ mice showed lipid-depleted BAT sections. During cold exposure, sympathetic stimulation of BAT increases *Dio2* expression and raises intracellular $T_3$ content that, in turn, stimulates

 

thermogenesis by increasing *Ucp1* transcription/stabilization and lipid metabolism [18]. In this context, we detected higher circulating $T_3$ levels in the WT and SIRT1$^{Tg+}$ mice after cold exposure. Although LPS impairs thyroid function, decreasing serum $T_3$, $T_4$, and TSH [106–109], SIRT1 has been described on the one hand to activate THs receptor β1 in the liver [110] and, on the other hand, to mediate a positive regulation of TSH secretion [111]. In this regard, we found a decline in $T_3$ and $T_4$ levels in the mice from both genotypes challenged with LPS and cold; this effect was attenuated in the SIRT1$^{Tg+}$ mice that preserved higher intra-BAT $T_3$ levels and this might be responsible, at least in part, for the beneficial effects observed in the thermogenic-related parameters studied and previously discussed. Altogether, our results demonstrate the specific relevance of $T_3$, which was enriched in medium 2, in the SIRT1$^{Tg+}$ mice rather than insulin since those mice showed similar circulating insulin levels as the WT [34,36]. These results were also supported by the rescue of the decline in UCP-1 levels in *db/db* mice treated with resveratrol as recently reported by Hui *et al.* [112] and also found in our study, likely related to the elevation in *Dio2* isoform that converts local $T_4$ to $T_3$ in BAT tissue [113] as well as increased *Fgf21* expression.

## 5. CONCLUSIONS

Hypothyroid patients showed decreased adaptive thermogenesis during cold exposure that was corrected by thyroid hormone replacement [114]. Thus, this study's results might have a translational impact on the treatment of obesity and other metabolic diseases, suggesting the use of combinatorial therapies of BAT-specific thyromimetics, with potentially fewer side effects than THs, along with SIRT1 activators.

## AUTHOR CONTRIBUTIONS

C.E. and P.V. participated in the study design, acquisition, analysis, data interpretation, and writing the manuscript. P.M. and S.Z. contributed to the Seahorse analysis and FAO experiments. E.G-C. contributed to characterization of the BA cell lines. A.M-*P. and* A.G.-F. performed the THs determinations. F.R.-S. and F.J.R. conducted the metabolomics analysis. D.S. and L.H. contributed to the Seahorse and FAO data analysis and discussion of the results. M.J.O. participated in the study design and data interpretation. A.M.V. participated in the study design and coordination and writing the manuscript. All the authors reviewed the manuscript and approved the final version.

## ACKNOWLEDGMENTS

This study was funded by grants RTI2018-094052-B-100 (MICINN/AEI/FEDER, EU), S2017/BMD-3684 (Community of Madrid, Spain), the Ramón Areces Foundation (Spain), and CIBERdem (ISCIII) to A.M.V., grant S2010/BMD-2423 (Community of Madrid, Spain) to M.J.O. and A.M.V., grants SAF2017-83813-C3-1-R (MICINN/AEI/FEDER, EU) and CIBERobn (grant CB06/03/0001, ISCIII, Spain) to L.H. and D.S., grants 2017SGR278 (Government of Catalonia) and 201627-30 (Fundació La Marató of TV3) to D.S., grant RTI2018-095166-B-I00 (MICINN/AEI/FEDER, EU) to F.J.R., and grants SAF2017-86342-R (MICINN/AEI/FEDER, EU) and CIBERer (ISCIII, Spain) to A.G.-F. C.E. is a recipient of an FPU fellowship (Ministry of Universities, Spain) (FPU 15/00251). S.Z. is a recipient of an ANID fellowship from Chile. We acknowledge the technical assistance of Laura Garcia, Noemi Alvarez, and Ariadna Segú. We acknowledge Miguel López (USC, Spain) for critically reading the manuscript and his comments and suggestions. We also acknowledge all the members of A.M.V.'s laboratory for helpful discussions.

## CONFLICT OF INTEREST

The authors declare no competing interests.

## APPENDIX A. SUPPLEMENTARY DATA

Supplementary data to this article can be found online at https://doi.org/10.1016/j.molmet.2020.101097.

## REFERENCES

[1] Catrysse, L., van Loo, G., 2017. Inflammation and the metabolic syndrome: the tissue-specific functions of NF-kappaB. Trends in Cell Biology 27(6): 417–429.

[2] Cannon, B., Nedergaard, J., 2004. Brown adipose tissue: function and physiological significance. Physiological Reviews 84(1):277–359.

[3] Caputo, T., Gilardi, F., Desvergne, B., 2017. From chronic overnutrition to metaflammation and insulin resistance: adipose tissue and liver contributions. FEBS Letters 591(19):3061–3088.

[4] Porter, C., 2017. Quantification of UCP1 function in human brown adipose tissue. Adipocyte 6(2):167–174.

[5] Nedergaard, J., Bengtsson, T., Cannon, B., 2007. Unexpected evidence for active brown adipose tissue in adult humans. American Journal of Physiology. Endocrinology and Metabolism 293(2):E444–E452.

[6] Cypess, A.M., Lehman, S., Williams, G., Tal, I., Rodman, D., Goldfine, A.B., et al., 2009. Identification and importance of brown adipose tissue in adult humans. New England Journal of Medicine 360(15):1509–1517.

[7] Virtanen, K.A., Lidell, M.E., Orava, J., Heglind, M., Westergren, R., Niemi, T., et al., 2009. Functional brown adipose tissue in healthy adults. New England Journal of Medicine 360(15):1518–1525.

[8] Cereijo, R., Gavaldà-Navarro, A., Cairó, M., Quesada-López, T., Villarroya, J., Morón-Ros, S., et al., 2018. CXCL14, a Brown adipokine that mediates Brown-Fat-to-Macrophage communication in thermogenic adaptation. Cell Metabolism 28(5):750–763.e756.

[9] Nisoli, E., Briscini, L., Giordano, A., Tonello, C., Wiesbrock, S.M., Uysal, K.T., et al., 2000. Tumor necrosis factor alpha mediates apoptosis of brown adipocytes and defective brown adipocyte function in obesity. Proceedings of the National Academy of Sciences of the United States of America 97(14): 8033–8038.

[10] Roberts-Toler, C., O'Neill, B.T., Cypess, A.M., 2015. Diet-induced obesity causes insulin resistance in mouse brown adipose tissue. Obesity 23(9): 1765–1770.

[11] Alcalá, M., Calderon-Dominguez, M., Bustos, E., Ramos, P., Casals, N., Serra, D., et al., 2017. Increased inflammation, oxidative stress and mitochondrial respiration in brown adipose tissue from obese mice. Scientific Reports 7(1), 16082-16082.

[12] Sakamoto, T., Nitta, T., Maruno, K., Yeh, Y.S., Kuwata, H., Tomita, K., et al., 2016. Macrophage infiltration into obese adipose tissues suppresses the induction of UCP1 level in mice. American Journal of Physiology. Endocrinology and Metabolism 310(8):e676–e687.

[13] Cannon, B., Nedergaard, J., 2011. Nonshivering thermogenesis and its adequate measurement in metabolic studies. Journal of Experimental Biology 214(Pt 2):242–253.

[14] Villarroya, J., Cereijo, R., Villarroya, F., 2013. An endocrine role for brown adipose tissue? American Journal of Physiology. Endocrinology and Metabolism 305(5):E567–E572.

[15] Villarroya, J., Cereijo, R., Gavalda-Navarro, A., Peyrou, M., Giralt, M., Villarroya, F., 2019. New insights into the secretory functions of brown adipose tissue. Journal of Endocrinology.

 

[16] Stanford, K.I., Middelbeek, R.J., Townsend, K.L., An, D., Nygaard, E.B., Hitchcox, K.M., et al., 2013. Brown adipose tissue regulates glucose homeostasis and insulin sensitivity. Journal of Clinical Investigation 123(1): 215–223.

[17] Bianco, A.C., Sheng, X.Y., Silva, J.E., 1988. Triiodothyronine amplifies norepinephrine stimulation of uncoupling protein gene transcription by a mechanism not requiring protein synthesis. Journal of Biological Chemistry 263(34):18168–18175.

[18] de Jesus, L.A., Carvalho, S.D., Ribeiro, M.O., Schneider, M., Kim, S.W., Harney, J.W., et al., 2001. The type 2 iodothyronine deiodinase is essential for adaptive thermogenesis in brown adipose tissue. Journal of Clinical Investigation 108(9):1379–1385.

[19] Ribeiro, M.O., Bianco, S.D., Kaneshige, M., Schultz, J.J., Cheng, S.Y., Bianco, A.C., et al., 2010. Expression of uncoupling protein 1 in mouse brown adipose tissue is thyroid hormone receptor-beta isoform specific and required for adaptive thermogenesis. Endocrinology 151(1):432–440.

[20] Martinez de Mena, R., Scanlan, T.S., Obregon, M.J., 2010. The T3 receptor beta1 isoform regulates UCP1 and D2 deiodinase in rat brown adipocytes. Endocrinology 151(10):5074–5083.

[21] Lowell, B.B., Spiegelman, B.M., 2000. Towards a molecular understanding of adaptive thermogenesis. Nature 404(6778):652–660.

[22] Guilherme, A., Yenilmez, B., Bedard, A.H., Henriques, F., Liu, D., Lee, A., et al., 2020. Control of adipocyte thermogenesis and lipogenesis through beta3-adrenergic and thyroid hormone signal integration. Cell Reports 31(5): 107598.

[23] Lin, J.Z., Martagon, A.J., Cimini, S.L., Gonzalez, D.D., Tinkey, D.W., Biter, A., et al., 2015. Pharmacological activation of thyroid hormone receptors elicits a functional conversion of white to Brown fat. Cell Reports 13(8):1528–1537.

[24] Yau, W.W., Singh, B.K., Lesmana, R., Zhou, J., Sinha, R.A., Wong, K.A., et al., 2019. Thyroid hormone (T3) stimulates brown adipose tissue activation via mitochondrial biogenesis and MTOR-mediated mitophagy. Autophagy 15(1): 131–150.

[25] Feingold, K., Kim, M.S., Shigenaga, J., Moser, A., Grunfeld, C., 2004. Altered expression of nuclear hormone receptors and coactivators in mouse heart during the acute-phase response. American Journal of Physiology. Endocrinology and Metabolism 286(2):E201–E207.

[26] Castro, I., Quisenberry, L., Calvo, R.M., Obregon, M.J., Lado-Abeal, J., 2013. Septic shock non-thyroidal illness syndrome causes hypothyroidism and conditions for reduced sensitivity to thyroid hormone. Journal of Molecular Endocrinology 50(2):255–266.

[27] de Vries, E.M., Fliers, E., Boelen, A., 2015. The molecular basis of the non-thyroidal illness syndrome. Journal of Endocrinology 225(3):R67–R81.

[28] Canto, C., Menzies, K.J., Auwerx, J., 2015. NAD(+) metabolism and the control of energy homeostasis: a balancing act between mitochondria and the nucleus. Cell Metabolism 22(1):31–53.

[29] Kupis, W., Pałyga, J., Tomal, E., Niewiadomska, E., 2016. The role of sirtuins in cellular homeostasis. Journal of Physiology and Biochemistry 72(3):371–380.

[30] Singh, C.K., Chhabra, G., Ndiaye, M.A., Garcia-Peterson, L.M., Mack, N.J., Ahmad, N., 2018. The role of sirtuins in antioxidant and redox signaling. Antioxidants and Redox Signaling 28(8):643–661.

[31] Nogueiras, R., Habegger, K.M., Chaudhary, N., Finan, B., Banks, A.S., Dietrich, M.O., et al., 2012. Sirtuin 1 and sirtuin 3: physiological modulators of metabolism. Physiological Reviews 92(3):1479–1514.

[32] Hubbard, B.P., Sinclair, D.A., 2014. Small molecule SIRT1 activators for the treatment of aging and age-related diseases. Trends in Pharmacological Sciences 35(3):146–154.

[33] Pfluger, P.T., Herranz, D., Velasco-Miguel, S., Serrano, M., Tschop, M.H., 2008. Sirt1 protects against high-fat diet-induced metabolic damage. Proceedings of the National Academy of Sciences of the United States of America 105(28):9793–9798.

[34] Banks, A.S., Kon, N., Knight, C., Matsumoto, M., Gutiérrez-Juárez, R., Rossetti, L., et al., 2008. SirT1 gain of function increases energy efficiency and prevents diabetes in mice. Cell Metabolism 8(4):333–341.

[35] Qiang, L., Wang, L., Kon, N., Zhao, W., Lee, S., Zhang, Y., et al., 2012. Brown remodeling of white adipose tissue by SirT1-dependent deacetylation of Ppargamma. Cell 150(3):620–632.

[36] Boutant, M., Joffraud, M., Kulkarni, S.S., Garcia-Casarrubios, E., Garcia-Roves, P.M., Ratajczak, J., et al., 2015. SIRT1 enhances glucose tolerance by potentiating brown adipose tissue function. Molecular Metabolism 4(2):118–131.

[37] Xu, F., Zheng, X., Lin, B., Liang, H., Cai, M., Cao, H., et al., 2016. Diet-induced obesity and insulin resistance are associated with brown fat degeneration in SIRT1-deficient mice. Obesity 24(3):634–642.

[38] Gonzalez-Rodriguez, A., Santamaria, B., Mas-Gutierrez, J.A., Rada, P., Fernandez-Millan, E., Pardo, V., et al., 2015. Resveratrol treatment restores peripheral insulin sensitivity in diabetic mice in a sirt1-independent manner. Molecular Nutrition & Food Research 59(8):1431–1442.

[39] Sun, C., Zhang, F., Ge, X., Yan, T., Chen, X., Shi, X., et al., 2007. SIRT1 improves insulin sensitivity under insulin-resistant conditions by repressing PTP1B. Cell Metabolism 6(4):307–319.

[40] Morreale de Escobar, G., Pastor, R., Obregon, M.J., Escobar del Rey, F., 1985. Effects of maternal hypothyroidism on the weight and thyroid hormone content of rat embryonic tissues, before and after onset of fetal thyroid function. Endocrinology 117(5):1890–1900.

[41] Obregon, M.J., Morreale de Escobar, G., Escobar del Rey, F., 1978. Concentrations of triiodo-L-thyronine in the plasma and tissues of normal rats, as determined by radioimmunoassay: comparison with results obtained by an isotopic equilibrium technique. Endocrinology 103(6):2145–2153.

[42] Weeke, J., Orskov, H., 1973. Synthesis of 125I monolabelled 3, 5, 3'-triiodothyronine and thyroxine of maximum specific activity for radioimmunoassay. Scandinavian Journal of Clinical & Laboratory Investigation 32(4): 357–360.

[43] Bárez-López, S., Grijota-Martínez, C., Ausó, E., Fernández-de Frutos, M., Montero-Pedrazuela, A., Guadaño-Ferraz, A., 2019. Adult mice lacking Mct8 and Dio2 proteins present alterations in peripheral thyroid hormone levels and severe brain and motor skill impairments. Thyroid : Official Journal of the American Thyroid Association 29(11):1669–1682.

[44] Quesada-Lopez, T., Cereijo, R., Turatsinze, J.V., Planavila, A., Cairo, M., Gavalda-Navarro, A., et al., 2016. The lipid sensor GPR120 promotes brown fat activation and FGF21 release from adipocytes. Nature Communications 7: 13479.

[45] Calderon-Dominguez, M., Alcala, M., Sebastian, D., Zorzano, A., Viana, M., Serra, D., et al., 2017. Brown adipose tissue bioenergetics: a new methodological approach. Advancement of Science 4(4):1600274.

[46] Herrero, L., Rubi, B., Sebastian, D., Serra, D., Asins, G., Maechler, P., et al., 2005. Alteration of the malonyl-CoA/carnitine palmitoyltransferase I interaction in the beta-cell impairs glucose-induced insulin secretion. Diabetes 54(2):462–471.

[47] Dalboge, L.S., Almholt, D.L., Neerup, T.S., Vassiliadis, E., Vrang, N., Pedersen, L., et al., 2013. Characterisation of age-dependent beta cell dynamics in the male db/db mice. PloS One 8(12):e82813.

[48] Burke, S.J., Batdorf, H.M., Burk, D.H., Noland, R.C., Eder, A.E., Boulos, M.S., et al., 2017. Db/db mice exhibit features of human type 2 diabetes that are not present in weight-matched C57BL/6J mice fed a western diet. Journal of Diabetes Research 2017:8503754.

[49] Belfiore, A., Malaguarnera, R., Vella, V., Lawrence, M.C., Sciacca, L., Frasca, F., et al., 2017. Insulin receptor isoforms in physiology and disease: an updated view. Endocrine Reviews 38(5):379–431.

[50] Cani, P.D., Bibiloni, R., Knauf, C., Waget, A., Neyrinck, A.M., Delzenne, N.M., et al., 2008. Changes in gut microbiota control metabolic endotoxemia-

 

induced inflammation in high-fat diet-induced obesity and diabetes in mice. Diabetes 57(6):1470—1481.

[51] Oh, D.Y., Morinaga, H., Talukdar, S., Bae, E.J., Olefsky, J.M., 2012. Increased macrophage migration into adipose tissue in obese mice. Diabetes 61(2): 346—354.

[52] Festuccia, W.T., Blanchard, P.-G., Deshaies, Y., 2011. Control of Brown adipose tissue glucose and lipid metabolism by PPARγ. Frontiers in Endocrinology 2, 84-84.

[53] Gereben, B., Zavacki, A.M., Ribich, S., Kim, B.W., Huang, S.A., Simonides, W.S., et al., 2008. Cellular and molecular basis of deiodinase-regulated thyroid hormone signaling. Endocrine Reviews 29(7):898—938.

[54] Kang, H., Oka, S., Lee, D.Y., Park, J., Aponte, A.M., Jung, Y.S., et al., 2017. Sirt1 carboxyl-domain is an ATP-repressible domain that is transferrable to other proteins. Nature Communications 8:15560.

[55] Liu, P.S., Wang, H., Li, X., Chao, T., Teav, T., Christen, S., et al., 2017. alpha-ketoglutarate orchestrates macrophage activation through metabolic and epigenetic reprogramming 18(9):985—994.

[56] Keiran, N., Ceperuelo-Mallafre, V., Calvo, E., Hernandez-Alvarez, M.I., Ejarque, M., Nunez-Roa, C., et al., 2019. SUCNR1 controls an anti-inflammatory program in macrophages to regulate the metabolic response to obesity 20(5):581—592.

[57] Bouter, B., Geary, N., Langhans, W., Asarian, L., 2010. Diet-genotype interactions in the early development of obesity and insulin resistance in mice with a genetic deficiency in tumor necrosis factor-alpha. Metabolism 59(7): 1065—1073.

[58] Tzanavari, T., Giannogonas, P., Karalis, K.P., 2010. TNF-alpha and obesity. Current Directions in Autoimmunity 11:145—156.

[59] Klover, P.J., Clementi, A.H., Mooney, R.A., 2005. Interleukin-6 depletion selectively improves hepatic insulin action in obesity. Endocrinology 146(8): 3417—3427.

[60] Matsubara, T., Mita, A., Minami, K., Hosooka, T., Kitazawa, S., Takahashi, K., et al., 2012. PGRN is a key adipokine mediating high fat diet-induced insulin resistance and obesity through IL-6 in adipose tissue. Cell Metabolism 15(1): 38—50.

[61] Escribano, O., Guillen, C., Nevado, C., Gomez-Hernandez, A., Kahn, C.R., Benito, M., 2009. Beta-Cell hyperplasia induced by hepatic insulin resistance: role of a liver-pancreas endocrine axis through insulin receptor A isoform. Diabetes 58(4):820—828.

[62] Huang, Z., Bodkin, N.L., Ortmeyer, H.K., Hansen, B.C., Shuldiner, A.R., 1994. Hyperinsulinemia is associated with altered insulin receptor mRNA splicing in muscle of the spontaneously obese diabetic rhesus monkey. Journal of Clinical Investigation 94(3):1289—1296.

[63] Starr, M.E., Evers, B.M., Saito, H., 2009. Age-associated increase in cytokine production during systemic inflammation: adipose tissue as a major source of IL-6. Journals of Gerontology Series A: Biological and Medical Sciences 64(7): 723—730.

[64] Rubio, C., Puerto, M., García-Rodríquez, J.J., Lu, V.B., García-Martínez, I., Alén, R., et al., 2020. Impact of global PTP1B deficiency on the gut barrier permeability during NASH in mice. Molecular Metabolism 35:100954.

[65] Zick, Y., 2005. Ser/Thr phosphorylation of IRS proteins: a molecular basis for insulin resistance. Science's STKE 2005(268):pe4.

[66] Sabio, G., Das, M., Mora, A., Zhang, Z., Jun, J.Y., Ko, H.J., et al., 2008. A stress signaling pathway in adipose tissue regulates hepatic insulin resistance. Science 322(5907):1539—1543.

[67] Ota, T., 2014. Obesity-induced inflammation and insulin resistance. Frontiers in Endocrinology 5, 204-204.

[68] Fu, C., Hao, S., Xu, X., Zhou, J., Liu, Z., Lu, H., et al., 2019. Activation of SIRT1 ameliorates LPS-induced lung injury in mice via decreasing endothelial tight junction permeability. Acta Pharmacologica Sinica 40(5):630—641.

[69] Lee, J.H., Moon, J.H., Lee, Y.J., Park, S.Y., 2017. SIRT1, a class III histone deacetylase, regulates LPS-induced inflammation in human keratinocytes and mediates the anti-inflammatory effects of hinokitiol. Journal of Investigative Dermatology 137(6):1257—1266.

[70] Zhang, W., Zhang, Y., Guo, X., Zeng, Z., Wu, J., Liu, Y., et al., 2017. Sirt1 protects endothelial cells against LPS-induced barrier dysfunction. Oxidative medicine and cellular longevity 2017, 4082102-4082102.

[71] Gariani, K., Menzies, K.J., Ryu, D., Wegner, C.J., Wang, X., Ropelle, E.R., et al., 2016. Eliciting the mitochondrial unfolded protein response by nicotinamide adenine dinucleotide repletion reverses fatty liver disease in mice. Hepatology 63(4):1190—1204.

[72] Lu, J., Zhang, L., Chen, X., Lu, Q., Yang, Y., Liu, J., et al., 2014. SIRT1 counteracted the activation of STAT3 and NF-kappaB to repress the gastric cancer growth. International Journal of Clinical and Experimental Medicine 7(12):5050—5058.

[73] Emanuelli, B., Peraldi, P., Filloux, C., Sawka-Verhelle, D., Hilton, D., Van Obberghen, E., 2000. SOCS-3 is an insulin-induced negative regulator of insulin signaling. Journal of Biological Chemistry 275(21):15985—15991.

[74] Liu, Z., Gan, L., Zhou, Z., Jin, W., Sun, C., 2015. SOCS3 promotes inflammation and apoptosis via inhibiting JAK2/STAT3 signaling pathway in 3T3-L1 adipocyte. Immunobiology 220(8):947—953.

[75] Shi, H., Tzameli, I., Bjorbaek, C., Flier, J.S., 2004. Suppressor of cytokine signaling 3 is a physiological regulator of adipocyte insulin signaling. Journal of Biological Chemistry 279(33):34733—34740.

[76] Stouthard, J.M., Oude Elferink, R.P., Sauerwein, H.P., 1996. Interleukin-6 enhances glucose transport in 3T3-L1 adipocytes. Biochemical and Biophysical Research Communications 220(2):241—245.

[77] Carey, A.L., Steinberg, G.R., Macaulay, S.L., Thomas, W.G., Holmes, A.G., Ramm, G., et al., 2006. Interleukin-6 increases insulin-stimulated glucose disposal in humans and glucose uptake and fatty acid oxidation in vitro via AMP-activated protein kinase. Diabetes 55(10):2688—2697.

[78] Hahn, W.S., Kuzmicic, J., Burrill, J.S., Donoghue, M.A., Foncea, R., Jensen, M.D., et al., 2014. Proinflammatory cytokines differentially regulate adipocyte mitochondrial metabolism, oxidative stress, and dynamics. American Journal of Physiology. Endocrinology and Metabolism 306(9):E1033—E1045.

[79] Zambrano, A., Molt, M., Uribe, E., Salas, M., 2019. Glut 1 in cancer cells and the inhibitory action of resveratrol as A potential therapeutic strategy. International Journal of Molecular Sciences 20(13):3374.

[80] Rotter, V., Nagaev, I., Smith, U., 2003. Interleukin-6 (IL-6) induces insulin resistance in 3T3-L1 adipocytes and is, like IL-8 and tumor necrosis factor-alpha, overexpressed in human fat cells from insulin-resistant subjects. Journal of Biological Chemistry 278(46):45777—45784.

[81] Albert, V., Svensson, K., Shimobayashi, M., Colombi, M., Munoz, S., Jimenez, V., et al., 2016. mTORC2 sustains thermogenesis via Akt-induced glucose uptake and glycolysis in brown adipose tissue. EMBO Molecular Medicine 8(3):232—246.

[82] Yoshizaki, T., Milne, J.C., Imamura, T., Schenk, S., Sonoda, N., Babendure, J.L., et al., 2009. SIRT1 exerts anti-inflammatory effects and improves insulin sensitivity in adipocytes. Molecular and Cellular Biology 29(5):1363—1374.

[83] Chen, S., Zhao, Z., Ke, L., Li, Z., Li, W., Zhang, Z., et al., 2018. Resveratrol improves glucose uptake in insulin-resistant adipocytes via Sirt1. The Journal of Nutritional Biochemistry 55:209—218.

[84] Gerhart-Hines, Z., Dominy Jr., J.E., Blattler, S.M., Jedrychowski, M.P., Banks, A.S., Lim, J.H., et al., 2011. The cAMP/PKA pathway rapidly activates SIRT1 to promote fatty acid oxidation independently of changes in NAD(+). Molecular Cell 44(6):851—863.

[85] Bordone, L., Cohen, D., Robinson, A., Motta, M.C., van Veen, E., Czopik, A., et al., 2007. SIRT1 transgenic mice show phenotypes resembling calorie restriction. Aging Cell 6(6):759—767.

[86] Xu, C., Bai, B., Fan, P., Cai, Y., Huang, B., Law, I.K., et al., 2013. Selective overexpression of human SIRT1 in adipose tissue enhances energy

 

homeostasis and prevents the deterioration of insulin sensitivity with ageing in mice. Journal Translational Research 5(4):412—426.

[87] Nohr, M.K., Bobba, N., Richelsen, B., Lund, S., Pedersen, S.B., 2017. Inflammation downregulates UCP1 expression in Brown adipocytes potentially via SIRT1 and DBC1 interaction. International Journal of Molecular Sciences 18(5).

[88] Li, X., 2013. SIRT1 and energy metabolism. Acta Biochimica et Biophysica Sinica 45(1):51—60.

[89] Goto, T., Naknukool, S., Yoshitake, R., Hanafusa, Y., Tokiwa, S., Li, Y., et al., 2016. Proinflammatory cytokine interleukin-1beta suppresses cold-induced thermogenesis in adipocytes. Cytokine 77:107—114.

[90] Shen, Z., Ajmo, J.M., Rogers, C.Q., Liang, X., Le, L., Murr, M.M., et al., 2009. Role of SIRT1 in regulation of LPS- or two ethanol metabolites-induced TNF-alpha production in cultured macrophage cell lines. American Journal of Physiology. Gastrointestinal and Liver Physiology 296(5): G1047—G1053.

[91] Wang, R., Dong, Z., Lan, X., Liao, Z., Chen, M., 2019. Sweroside alleviated LPS-induced inflammation via SIRT1 mediating NF-kappaB and FOXO1 signaling pathways in RAW264.7 cells. Molecules 24(5).

[92] Zhang, H., Shan, Y., Wu, Y., Xu, C., Yu, X., Zhao, J., et al., 2017. Berberine suppresses LPS-induced inflammation through modulating Sirt1/NF-kappaB signaling pathway in RAW264.7 cells. International Immunopharmacology 52:93—100.

[93] Nguyen, K.D., Qiu, Y., Cui, X., Goh, Y.P., Mwangi, J., David, T., et al., 2011. Alternatively activated macrophages produce catecholamines to sustain adaptive thermogenesis. Nature 480(7375):104—108.

[94] Sarjeant, K., Stephens, J.M., 2012. Adipogenesis. Cold Spring Harbor perspectives in biology 4(9) a008417-a008417.

[95] Kajimura, S., Seale, P., Spiegelman, B.M., 2010. Transcriptional control of brown fat development. Cell Metabolism 11(4):257—262.

[96] Lee, J.H., Park, A., Oh, K.-J., Lee, S.C., Kim, W.K., Bae, K.-H., 2019. The role of adipose tissue mitochondria: regulation of mitochondrial function for the treatment of metabolic diseases. International Journal of Molecular Sciences 20(19):4924.

[97] Pisani, D.F., Barquissau, V., Chambard, J.-C., Beuzelin, D., Ghandour, R.A., Giroud, M., et al., 2018. Mitochondrial fission is associated with UCP1 activity in human brite/beige adipocytes. Molecular metabolism 7:35—44.

[98] Wikstrom, J.D., Mahdaviani, K., Liesa, M., Sereda, S.B., Si, Y., Las, G., et al., 2014. Hormone-induced mitochondrial fission is utilized by brown adipocytes as an amplification pathway for energy expenditure. The EMBO Journal 33(5): 418—436.

[99] Yang, S.J., Choi, J.M., Chang, E., Park, S.W., Park, C.Y., 2014. Sirt1 and Sirt6 mediate beneficial effects of rosiglitazone on hepatic lipid accumulation. PloS One 9(8):e105456.

[100] Ohno, H., Shinoda, K., Spiegelman, B.M., Kajimura, S., 2012. PPARgamma agonists induce a white-to-brown fat conversion through stabilization of PRDM16 protein. Cell Metabolism 15(3):395—404.

[101] Nilsson, N.O., Stralfors, P., Fredrikson, G., Belfrage, P., 1980. Regulation of adipose tissue lipolysis: effects of noradrenaline and insulin on phosphorylation of hormone-sensitive lipase and on lipolysis in intact rat adipocytes. FEBS Letters 111(1):125—130.

[102] Mills, E.L., Pierce, K.A., Jedrychowski, M.P., Garrity, R., Winther, S., Vidoni, S., et al., 2018. Accumulation of succinate controls activation of adipose tissue thermogenesis. Nature 560(7716):102—106.

[103] Croze, M.L., Vella, R.E., Pillon, N.J., Soula, H.A., Hadji, L., Guichardant, M., et al., 2013. Chronic treatment with myo-inositol reduces white adipose tissue accretion and improves insulin sensitivity in female mice. The Journal of Nutritional Biochemistry 24(2):457—466.

[104] Lopez, M., Varela, L., Vazquez, M.J., Rodriguez-Cuenca, S., Gonzalez, C.R., Velagapudi, V.R., et al., 2010. Hypothalamic AMPK and fatty acid metabolism mediate thyroid regulation of energy balance. Nature Medicine 16(9):1001—1008.

[105] Martinez-Sanchez, N., Seoane-Collazo, P., Contreras, C., Varela, L., Villarroya, J., Rial-Pensado, E., et al., 2017. Hypothalamic AMPK-ER stress-JNK1 Axis mediates the central actions of thyroid hormones on energy balance. Cell Metabolism 26(1):212—229.e212.

[106] Iaglova, N.V., Berezov, T.T., 2010. [Regulation of thyroid and pituitary functions by lipopolysaccharide]. Biomed Khim 56(2):179—186.

[107] Beigneux, A.P., Moser, A.H., Shigenaga, J.K., Grunfeld, C., Feingold, K.R., 2003. Sick euthyroid syndrome is associated with decreased TR expression and DNA binding in mouse liver. American Journal of Physiology. Endocrinology and Metabolism 284(1):E228—E236.

[108] Boelen, A., Kwakkel, J., Thijssen-Timmer, D.C., Alkemade, A., Fliers, E., Wiersinga, W.M., 2004. Simultaneous changes in central and peripheral components of the hypothalamus-pituitary-thyroid axis in lipopolysaccharide-induced acute illness in mice. Journal of Endocrinology 182(2):315—323.

[109] Kondo, K., Harbuz, M.S., Levy, A., Lightman, S.L., 1997. Inhibition of the hypothalamic-pituitary-thyroid Axis in response to lipopolysaccharide is independent of changes in circulating corticosteroids. Neuroimmunomodulation 4(4):188—194.

[110] Suh, J.H., Sieglaff, D.H., Zhang, A., Xia, X., Cvoro, A., Winnier, G.E., et al., 2013. SIRT1 is a direct coactivator of thyroid hormone receptor β1 with gene-specific actions. PloS One 8(7) e70097-e70097.

[111] Akieda-Asai, S., Zaima, N., Ikegami, K., Kahyo, T., Yao, I., Hatanaka, T., et al., 2010. SIRT1 regulates thyroid-stimulating hormone release by enhancing PIP5Kgamma activity through deacetylation of specific lysine residues in mammals. PloS One 5(7):e11755.

[112] Hui, S., Liu, Y., Huang, L., Zheng, L., Zhou, M., Lang, H., et al., 2020. Resveratrol enhances brown adipose tissue activity and white adipose tissue browning in part by regulating bile acid metabolism via gut microbiota remodeling. International Journal of Obesity.

[113] Bianco, A.C., Kim, B.W., 2006. Deiodinases: implications of the local control of thyroid hormone action. Journal of Clinical Investigation 116(10):2571—2579.

[114] Broeders, E.P., Vijgen, G.H., Havekes, B., Bouvy, N.D., Mottaghy, F.M., Kars, M., et al., 2016. Thyroid hormone activates Brown adipose tissue and increases non-shivering thermogenesis–A cohort study in a group of thyroid carcinoma patients. PloS One 11(1):e0145049.

 